CHALMERS
UNIVERSITY OF TECHNOLOGY

Optimal predictive control applied to thermal management of electrified heavy vehicles

Physical modelling for the thermal system of a battery electric vehicle for simulating a receding horizon controller

Master's thesis in Systems, control & mechatronics

MAX LILJEQVIST

DEPARTMENT OF ELECTRICAL ENGINEERING

CHALMERS UNIVERSITY OF TECHNOLOGY
Gothenburg, Sweden 2023
www.chalmers.se

Master's thesis 2023

Optimal predictive control applied to thermal management of electrified heavy vehicles

Physical modelling for the thermal system of a battery electric vehicle for simulating a receding horizon controller.

MAX LILJEQVIST

CHALMERS
UNIVERSITY OF TECHNOLOGY

Department of Electrical Engineering
Division of Systems and control
Chalmers University of Technology
Gothenburg, Sweden 2023

Optimal predictive control applied to thermal management of electrified heavy vehicles
Physical modelling for the thermal system of a battery electric vehicle for simulating a receding horizon controller
MAX LILJEQVIST

Supervisor: Olof Lindgärde, AB Volvo
Examiner: Torsten Wik, Head of Unit at Systems and Control

Master's Thesis 2023
Department of Electrical Engineering
Division of Systems and control
Chalmers University of Technology
SE-412 96 Gothenburg
Telephone +46 31 772 1000

Cover: A heavy electrified vehicle with temperature state trajectories generated with Matlab in the background with a color gradient.

Typeset in LaTeX
Printed by Chalmers Reproservice
Gothenburg, Sweden 2023

Optimal predictive control applied to thermal management of electrified heavy vehicles
Physical modelling for the thermal system of a battery electric vehicle for simulating a receding horizon controller.
MAX LILJEQVIST
Department of Electrical Engineering
Chalmers University of Technology

Abstract

Battery electric vehicles (BEVs) are increasingly used for the electrification of the transport sector. It is of great importance to improve vehicle range and lifetime of system components to remain competitive and ensure customer satisfaction. Control strategies aimed at reducing overall energy usage and minimizing component wear are actively being researched. This thesis suggests and simulates a model-based receding horizon control strategy for the thermal system of a battery electric heavy duty truck. The objective is to track reference temperatures of the electric storage system (ESS) and motor drive systems (MDS) while minimizing actuator power, such as heat pumps, fans, the pumps and the valves. Particularly, there is a focus on the mathematical modelling of dynamic coupling between the thermal loops of the ESS and MDS. The system dynamics are captured using process engineering methods, including control volume analysis and heat exchanger modelling. The system has a high number of degrees of freedom. An optimal control problem is then formulated by utilizing the direct collocation method. Simulation results indicate that the final receding horizon controller improves energy usage as well as reference tracking performance by effectively anticipating future disturbances. While there is potential for developing more accurate system models compared to the real-life system, the suggested control structure is a solid foundation for future improvements.

Keywords: Battery electric vehicles, receding horizon control, thermal system, optimal control, heat transfer.

Acknowledgements

I will start by directing appreciation at and thanking Mohammad Abdollahpouri for initiating the idea for the thesis and deliberating how to approach the complex task. I would also like to thank Ashkan Ghodrati, Alessandro Capancioni and Adam Lagerberg for their support and feedback during the thesis work. I am also expressing great gratitude to Olof Lindgärde for taking over the role as supervisor and for the continuous feedback and discussions keeping me well on track to finish the thesis work.

I am also grateful for the insightful guidance provided by my examiner Torsten Wik. His expertise in the interdisciplinary field of process control, bridging the domains of control engineering and process engineering, helped me to navigate the complexities of the thesis work.

Max Liljeqvist, Gothenburg, June 2023

Contents

List of Figures

List of Acronyms

Below is the list of acronyms that have been used throughout this thesis listed in alphabetical order:

BEV	Battery Electric Vehicle
ESS	Electric Storage System
MDS	Motor Drive System
MPC	Model Predictive Control
NLP	Nonlinear Programming
NMPC	Nonlinear Model Predictive Control
NTU	Number of Transfer Units
OCP	Optimal Control Problem
RHC	Receding Horizon Control

Nomenclature

Below is the nomenclature of indices, sets, parameters, and variables that have been used throughout this thesis.

Indices

B	Index for variables and parameters concerning the ESS
M	Index for variables and parameters concerning the MDS
c	Index for variables and parameters concerning the coolant fluid
r	Index for variables and parameters concerning the radiator
env	Index for variables and parameters concerning the environment

Parameters

m_i	Mass of component i
ρ	Density of the coolant fluid
$C_{p,i}$	Specific heat capacity of i
α^i_{env}	Coefficient of heat transfer from i to environment
T_{amb}	Ambient temperature
ϵ_i	NTU method heat transfer effectiveness of i
C_i	Heat capacity rate of flow i
U	Overall heat transfer coefficient
Nu	Nusselt number
Re	Reynolds number
Pr	Prandtl number
v	Coolant fluid speed
μ	Coolant fluid dynamic viscosity
k	Coolant fluid thermal conductivity

D	Pipe diameter
$A_{\perp}$	Pipe cross-sectional area
V_i	Control volume of i
T	Prediction horizon
N	Number of horizon control points

Sets

x	state vector
u	input vector
d	disturbance vector
r	reference vector

Variables

T_i	Temperature of i
$\dot{T}_i$	Time derivative of temperature i
$\dot{Q}_{ESS},\ \dot{Q}_{MDS}$	Heat generation rate of ESS, MDS
$\dot{Q}_{cB},\ \dot{Q}_{cM}$	Heat transfer rate from ESS, MDS to coolant
$\dot{Q}^i_{env}$	Heat transfer rate from component i to the environment
$\dot{Q}_{ch}$	Heat transfer rate from the Heater/Chiller unit to coolant
ω_f	Fan revolutions per minute
$\dot{Q}_f$	Heat transfer rate from the Radiator & Fan to coolant
$f_B,\ f_M$	Volumetric flow of coolant fluid in the ESS, MDS loop
η_d	Valve decoupling position (0 to 1)
η_r	Radiator valve position (0 to 1)

1

Introduction

Predictive thermal management in electrified heavy vehicles is a control strategy that has potential to more efficiently utilize stored energy to meet temperature targets of vehicle components [1]. The thermal system in question includes two separate closed loops; one containing a battery along with a heater and chiller, and one loop with motor drive systems with a radiator-fan cooling unit which can be bypassed using a valve. The two loops are *decoupled* at standard operations, but can be connected together into a single continuous loop by switching two valves that share a binary variable (coupled or decoupled). The prospect of dynamically controlling the valves (along with other system parameters) with continuous signals in a receding horizon control strategy is to improve overall thermal performance. Receding horizon control allows for controlling a system with multiple variables and constraints by repeatedly simulating the future behavior of a system and its control signals based on a mathematical model. Therein were challenges in modelling and optimization to be solved. The final control system is not only applicable and useful for battery electric vehicles (BEVs), but could be expanded to incorporate cooling of hydrogen fuel cell systems. The use of hydrogen fuel cells is an emerging technology within the automotive industry presenting many opportunities for further development.

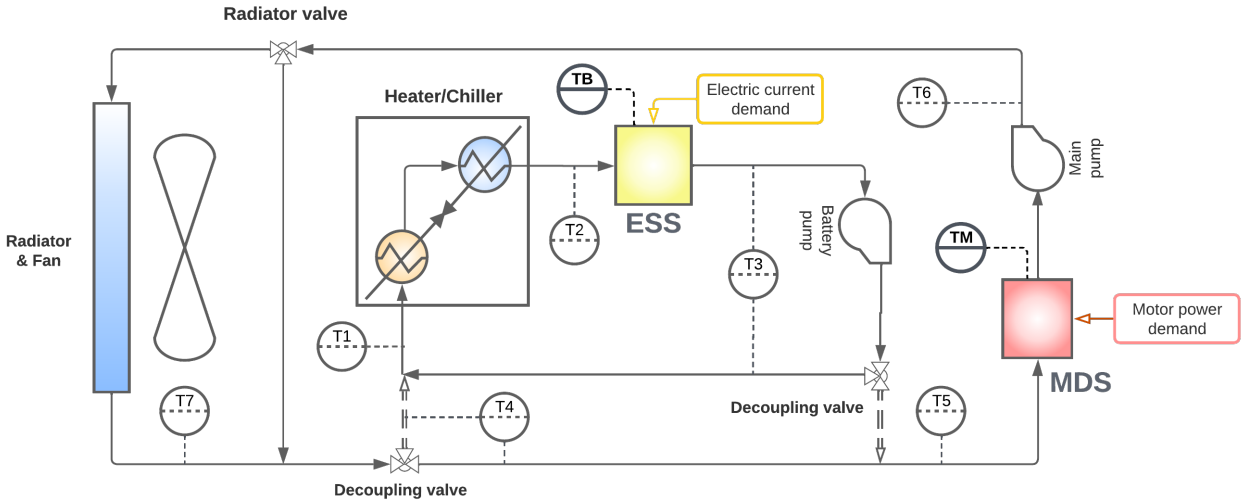

Figure 1.1: Thermal system with two main loops; the inner loop containing a heater/chiller unit with the electric storage system, and the outer loop consisting of the motor drive system with a cooling radiator/fan.

1.1 Motivation

The purpose of this work is to provide long term knowledge to academia and the company regarding modelling, optimization and control of the predictive thermal management system. The application of the receding horizon controller could imply reduced energy usage and battery wear in electrified heavy trucks [2]. This falls well into line with sustainability goals while also improving profitability and customer satisfaction.

1.2 Aim

The objective is to recreate a simplified version of the system by modelling to include dynamic valve switching (in practice extending the input vector and including more detailed system equations). The controller should be able to handle the more complicated dynamics while meeting the temperature demands on the battery as well as motor drive systems, compensating for disturbances in the form of vehicle power and speed trajectories. Two scenarios are possible; the decoupling valve variable is continuous between 0 and 1, or strictly binary. The first scenario is preferable but both scenarios would be improvements, because both loops could then be controlled by a single receding horizon controller.

The overall limitations of the work have been quite clear. The final receding horizon controller with dynamic valve coupling control was to be compared to the decoupled version of the system. The physical modelling did not need to go into too much detail. Instead more general expressions for the unit operations could be used, partly for saving time and partly for the optimization solver to work effectively. An example is the use of elementary heat transfer relations for the heat exchangers.

1.3 Background

Volvo is committed to the ambitions and climate change goals of the Paris Agreement. The transport industry is rapidly developing new technologies to meet customer demands regarding environmental impact while staying competitive. Relevant areas of study are the energy consumption efficiency and improvement of component lifetime in electrified heavy-duty trucks, which drives the industry to utilize advanced optimization methods.

Model based optimal predictive control is a well-established control methodology that has been proven efficient in industry and academia. Creating viable embeddable optimal control solution methods is a challenge despite significant research on the problem. There exist thermal management solutions that are computationally demanding, therefore the ambition of this thesis project is to define and design a feasible and controllable optimization problem that could be suitable for embedded software.

An optimal control problem can tackle a minimization problem while maintaining the limitations of the system in a unified solution. A balance between cooling performance and energy consumption is at the heart of the problem. It is desirable to use as little cooling power as possible while also keeping component temperatures as close to the reference values as possible. Including constraints means bounding the values to certain intervals. These can be hard constraints (cooling power being physically bounded by a cooling valve) and softer yet important constraints (temperatures of the battery packs should stay within specified bounds to not degrade lifetime of the components).

The main challenge is to define an optimal control problem that includes all relevant component requirements while targeting a desirable objective. Some constraints are simpler to implement, like the temperature and cooling power bounds. Others are less straight-forward to implement such as fan power consumption, the aging model of the batteries and the prediction of impending thermal load. Non-linearity in some of these terms are important to be reformulated in a way to keep the problem feasible and preferably convex. Complicating the control problem means increasing the computation resources needed, which should be kept low to better meet the potential limitations of the embedded hardware; this can be both in terms of memory and computational power limitation. Implementing an optimization based control system has the potential of reducing the overall energy consumption compared to traditional methods. It also has potential of improving the life-time of components. This means an increased range of the electric vehicle while providing increased life-time warranty to customers. Demonstrating a net decrease of energy usage by even a few percentages would be a substantial benefit for both the company and customers, and has been done by similar methods before [3].

1.4 Problem statement

After developing a mathematical model for the dynamic thermal system including system variables, control inputs and constraints, the goal of the receding horizon controller is to repeatedly calculate a sequence of optimal control inputs over a prediction horizon while minimizing a cost function. The cost function is an expression that consists of several terms that represent system performance, such as state reference tracking, control effort and terminal state values. Each term in the cost function is multiplied by specific scalar parameters known as tuning weights. Priority between system states and control signals can be adjusted individually, which means that system performance can be improved by changing the values of these tuning weights. The main research questions are then posed as:

- How to control the complete cooling system and thermal management for, e.g., motor drive system, battery packs, active/passive cooling component, pumps, and valves, in MATLAB in a receding horizon control strategy?
- How to address different cost terms in a balanced manner? For example, is it possible to convert all these terms in the same unit so that the tuning work is simplified?
- Some valves are on-off, and without over-complicating the problem (e.g., go-

ing into event-based optimal theory), is it possible to control the valves as continuous control signals?

1.5 Ethical considerations

The overall goal of electrification is to reduce reliance on non-renewable energy sources to limit net increase of carbon dioxide and other greenhouse gases in the atmosphere, which is in accordance with sustainable development goal 13. Of course, there are always challenges to overcome during technological paradigm shifts. Successfully meeting the goals of this thesis project advances the overall goal at Volvo to electrify the automotive industry, not to mention their industry position amid fierce competition. Electric vehicles are associated with several cons. A prominent issue is caused by life cycle the batteries themselves. Mining of natural resources, like lithium, impacts both the local environment and the climate [4]. Production of the batteries emits significant amounts of carbon dioxide if not based on fossil free electricity. There are also challenges to be considered regarding recycling of batteries.

Regarding UN's sustainable development goal 3, good health and well-being, electrified vehicles generally improve air quality of populated areas leading to better overall public health. Accidents, however, causing damage to electric vehicles are considered less safe to repair than petrol or diesel vehicles. Damaged batteries can behave unpredictably, posing risk of fire, explosion and high voltage discharge with potentially fatal consequences [5]. The aspect of quieter vehicles poses a similar perspective, reducing noise in urban areas contributes to better overall living. There are concerns that the silent nature of electric vehicles makes them harder to identify for pedestrians and other drivers, increasing risk of accidents [6].

Depending on the market situation, sustainable development goal 7 might not be improved. Electric vehicles significantly increase the demand for electricity. Without adequate expansion of clean and cheap electricity production, energy becomes less affordable and potentially dirtier. If, for example, increased electricity demand is met by establishing new coal and oil power plants then climate benefits of electric vehicles are actively hampered.

Improvement of electrified heavy vehicles would contribute to sustainable development goals 8 and 9 in a clear way. Electrification enables major work opportunities and economic growth by benefiting innovative industry [7]. In the Gothenburg metropolitan area, the automotive industry is a major part of the city's employment. Electrification is seeing growth in both the automotive industry and new industries for the area. Examples include battery manufacturing and electrified aircraft development. The overall benefits outweigh the challenges that vehicle electrification ultimately contribute towards.

2
Theory

2.1 The thermal system

The system that is considered contains two main loops; one loop for the ESS and one for the MDS (see Figure 1.1). In the standard decoupled mode these two loops can be regarded as two separate systems. The ESS loop has three main components: the ESS itself, the Heater/Chiller unit and the battery pump. The ESS temperature is then mainly controlled by the Heater/Chiller. The coolant in the ESS loop is assumed to have three temperature measuring positions T_1, T_2 and T_3. The MDS loop contains the MDS itself, the main pump, the Radiator & Fan unit and the radiator valve η_r (which can be used to bypass the radiator). The coolant is here assumed to have the temperature measuring positions T_4, T_5, T_6 and T_7.

The variable η_d that the two decoupling valves share is of special interest in the system because it combines the two separate loops ($\eta_d = 0$) into one greater continuous loop ($\eta_d = 1$).

2.2 Thermodynamics

The study of thermodynamics describes the fundamentals of energy transformations. Some basic knowledge of fields based on thermodynamics is helpful to follow modelling methods of the thermal system such as control volume analysis, heat generation and heat transfer. There are three laws of thermodynamics that are briefly stated before introducing the more in-depth methods:

- The first law of thermodynamics is also known as the conservation of energy principle; energy can neither be created nor destroyed, only transferred or converted to different forms [8]. This lays the foundation for energy balances which is a key concept in engineering and the most relevant law for the modelling work to follow.

- The second law of thermodynamics concerns entropy of a closed system, stating that the total entropy of the system will increase over time [8]. This can be thought of as a tendency of systems to become more disorderly or random. The law is important for concepts such as efficiency, describing why irreversible processes exist and perfect efficiency is impossible.

- The third law of thermodynamics states the impossibility of reaching absolute zero by a finite series of processes. A perfect crystal at absolute zero is zero. This law is of less relevance to the problem at hand but is of great importance for the fields of material science and quantum mechanics.

2.2.1 Control volume analysis

To model change in temperature over a region in space a *control volume* can be defined which is bounded by a control surface. The first law of thermodynamics can be applied to state that; change in stored energy must equal the amount of energy that enters the control volume minus energy that leaves the control volume [9]. This is also known as the conservation of energy requirement. For a generic case the types of energies considered are a sum of mechanical energies (potential and kinetic) and internal energies (e.g. thermal or chemical). An overall general energy balance can be mathematically stated as

$$\frac{\partial E}{\partial t} = \dot{m}(H + \frac{v^2}{2} + gz)_{in} - \dot{m}(H + \frac{v^2}{2} + gz)_{out} + q + q_{gen} - q_{con} - \dot{W}, \tag{2.1}$$

in the unit joules per second, where H is enthalpy, v is velocity, z is height, q is heat transferred, q_{gen} is heat generated, q_{con} is consumed heat and $\dot{W}$ is work done by the system. As is often the case several terms can be considered to be negligible depending on the problem statement at hand. For a system that is adiabatic (no heat transfer), with no heat being generated or consumed, where no work is done and mechanical energies can be neglected, the equation is simplified to

$$\frac{\partial E}{\partial t} = \dot{m}(H_{in} - H_{out}). \tag{2.2}$$

Assuming constant heat capacity the relation can be stated as

$$\frac{\partial E}{\partial t} = \dot{m}C_p(T_{in} - T_{out}) \tag{2.3}$$

which with a few variables exchanged ($\dot{m} = \rho f$, $\frac{\partial E}{\partial t} = \rho V C_p \dot{T}$) can be put into a form that will be important in the modelling of the thermal system:

$$\rho V C_p \dot{T} = \rho C_p(f_{in}T_{in} - f_{out}T_{out}), \tag{2.4}$$

where ρ is fluid density, f is volumetric flow and V is control volume.

2.2.2 Heat generation

Generation of heat comes in many forms. There are two of relevance to the thermal system at hand that will be described in some detail in this section; resistive heating and friction heating. Both of these forms of heat generation are directly related to the second law of thermodynamics.

The heat generation of the ESS is assumed to be resistive heat. The electrical energy of the ESS being lost as heat due to current flowing through resistive material is described by

$$\dot{Q}_{ESS} = RI^2, \tag{2.5}$$

where R is the resistance of the material (which may change with temperature) and I is the electric current. Increased current demand on the ESS also increases the heat generated.

The heat generation of the MDS is assumed to be caused by frictional heating. Friction between moving parts between surfaces in the MDS converts some of the useful mechanical energy to thermal energy. Mathematically this heat is proportional to some heat generation coefficient times the power demand of the MDS.

$$\dot{Q}_{MDS} = \alpha_F P_{MDS} \tag{2.6}$$

For the modelling, the two terms $\dot{Q}_{ESS}$ and $\dot{Q}_{MDS}$ are considered as system disturbances that the controller should alleviate to track the temperature setpoints.

2.2.3 Heat transfer

Heat transfer is a large field of science and engineering that can be very in-depth. This section will go into basic details to segue to the heat transfer methods. Heat transfer studies the movement of thermal energy, which at a macroscopic level concerns temperature differences. At a microscopic level this is caused by exchange of kinetic energy between molecules. The three modes of energy transfer are conduction, convection and radiation. In real problems all three often occur simultaneously [10].

- Conduction is transfer of heat through a stationary medium caused by differences in temperature between adjacent regions [10]. Kinetic energy from molecules of high temperature is transferred via collisions with lower temperature molecules. The general relation for conduction in a direction x is

  $$\dot{Q}_x = -kA\frac{dT}{dx} \tag{2.7}$$

  where $\dot{Q}_x$ is the heat flux, k is the thermal conductivity of the material, A the heat transfer area normal to x and $\dfrac{dT}{dx}$ is the temperature gradient in direction x.

- Convection is heat transferred between a moving fluid, such as a liquid or gas, and a surface [10]. The two ways are natural convection caused primarily by density differences, and forced convection, where the fluid is moved by an external source. The general relation for convective heat transfer is also known as the *Newton rate equation*:

$$\dot{Q} = hA\Delta T \tag{2.8}$$

where ΔT is the temperature difference between the surface and the fluid, A is the heat transfer area and h is the convective heat transfer coefficient. This coefficient is notoriously laborious to calculate as it depends on many factors including geometry of the system, fluid parameters, flow parameters and the temperature difference. There are numerous empirically derived relations for the calculation of h, but details of this will be described later in the report.

- Lastly, radiation is caused by heat by means of electromagnetic waves between surfaces [10]. Heat radiation depends on many material parameters such as absorptivity, emissivity and others. This mode of heat transfer is not of immediate relevance and will not be discussed in more detail.

2.2.4 Heat exchangers

A heat exchanger is a common practical application of heat transfer theory, yet the design of heat exchangers is very in-depth. Heat exchanger design concerns many aspects such as calculation of operating points (e.g. inlet and outlet temperatures, heat effect), heat exchanger area required, physical parameters, fluid configuration, geometry and cost targeting. These aspects depend on each other and the problems quickly become complex. The focus here is not on the heat exchanger models themselves and will therefore be kept relatively simple. Nonetheless, some theory of a basic single-pass heat exchanger will be described.

A basic heat exchanger setup is a single-pass exchanger between one hot stream (stream that needs cooling) and one cold stream (stream that needs heating). Single-pass means that the streams only pass each other once [11]. The heat transferred is

$$\dot{Q} = UA\Delta T_{lm}, \tag{2.9}$$

where U is the overall heat transfer coefficient, A is heat exchanger area and ΔT_{lm} is the logarithmic mean temperature. The overall heat transfer coefficient for the general case over a heat exchanger plate is

$$\frac{1}{U} = \frac{1}{h_c} + \frac{\delta}{k} + \frac{1}{h_h}, \tag{2.10}$$

where h_c and h_h are the convective heat transfer coefficients of the cold and hot side, respectively. The heat conduction is accounted for by the plate thickness δ and the conductivity k. In some cases these parameters vary enough to justify neglecting all but one. For example, neglecting the conduction resistance for a very thin plate. Sometimes either the cold or hot side convection resistance is much higher than the other, making the overall heat transfer limited to the slowest parameter.

Because the temperatures continuously change through the heat exchanger, the logarithmic mean temperature ΔT_{lm} is used to approximate the change in temperature difference between the streams:

$$\Delta T_{lm} = \frac{\Delta T_1 - \Delta T_2}{ln(\frac{\Delta T_1}{\Delta T_2})}. \tag{2.11}$$

with ΔT_1 being the temperature difference between the hot and cold stream on one side of the heat exchanger and ΔT_2 on the other [11]. This implies that for a nominal heat exchanger problem, four temperatures are needed for modelling. This can cleverly be reduced to two using the NTU method [12].

2.2.4.1 The NTU method

For the case where all inlet and outlet temperatures are known it is easy to utilize the logarithmic mean temperature. The NTU (*Number of transfer units*) or *effectiveness* method is preferable when only the inlet temperatures are known. The NTU method has effectively been used for modeling in control problems [13].

Consider the following definitions:

$$C_c = \dot{m}_c C_{p,c}, \quad C_h = \dot{m}_h C_{p,h}. \tag{2.12}$$

The effectiveness of a heat exchanger is derived from the maximum possible theoretical heat transferred

$$\dot{Q}_{max} = C_{min}(T_{h,in} - T_{c,in}), \tag{2.13}$$

where

$$C_{min} = min\{C_c, C_h\}. \tag{2.14}$$

The effectiveness term ϵ is defined as the quotient between the actual heat transfer and the theoretical maximum

$$\epsilon = \frac{\dot{Q}}{\dot{Q}_{max}}, \tag{2.15}$$

where $\dot{Q}$ is defined as

$$\dot{Q} = \epsilon C_{min}(T_{h,in} - T_{c,in}). \tag{2.16}$$

It can be shown that ϵ for any heat exchanger can be found by

$$\epsilon = f\left(NTU, C_r = \frac{C_{min}}{C_{max}}\right), \tag{2.17}$$

with NTU being a dimensionless number defined as

$$NTU = \frac{UA}{C_{min}}. \tag{2.18}$$

The actual relation between NTU and ϵ as in Equation 2.17 depends on stream and geometric configuration. A specially relevant case is when there is assumed to only be one stream ($C_r = 0$),

$$\epsilon = 1 - e^{-NTU}. \tag{2.19}$$

2.3 Mathematical optimization

Optimization is a mathematical field with very broad utilization, from economics to technical systems. It essentially is the science of calculating the best decision, given particular circumstances. The basis of entry to use mathematical optimization is that the problem can be formulated on a systematic form. The variables that can be manipulated are called *decision variables* [14]. To know the optimal choice of decision variables an objective has to be defined in an *objective function* to be maximized or minimized. Most problems include limitations on the decision variables, called *constraints*. The general mathematical formulation is

$$\begin{aligned} &\text{minimize} \quad f(\mathbf{x}) \\ &\text{such that} \quad g_i(\mathbf{x}) \leq b_i, \quad i = 1, ..., m. \end{aligned} \tag{2.20}$$

A brief introduction to some common types of optimization problems is made. This includes *linear programming* problems, *nonlinear programming* problems and *integer programming* problems. A problem is linear if all functions f and g are linear in x. It is nonlinear if *at least* one of the functions is nonlinear. If a subset of the decision variables are constrained to integer values it is an integer problem. Nonlinear and integer programming are associated with potentially much higher computation times than linear programming. Sometimes it is possible to cleverly simplify complex problems for better solver efficiency [15]. In this work, one of the overall aims is to avoid an integer programming problem by considering valve positions as continuous variables.

The process of identifying a real problem and then formulating a simplified mathematical formulation often poses a challenge [14]. The validity and relevance of the solved optimization problem depends on the detail of the formulation, which makes optimization an iterative process. There may be a conflict between the desired accuracy of the solution and the required resources to achieve it, such as the hours of engineering work and the computational resources.

2.4 Optimal control

The bridge between control theory and mathematical optimization is the optimization of dynamic systems, also known as *optimal control* [16]. Optimal control problems (OCP) are different from general optimization by incorporating differential equations into the formulation, which can be highly complex. Other control concepts, such as minimizing reference deviation, can readily be included in the objective function. The methods for solving these often include discretizing the problem. Some are based on discretize-then-optimize, and others on optimize-then-discretize, all-at-once or shooting-methods. A subsection of the available methods is will be detailed here, but the detailed procedure is described in the "Methods" chapter. The overall strategy is to formulate a continuous time optimal control problem, that is transformed to a nonlinear program to be solved using a collocation method. This is called a direct method [17].

2.4.0.1 Direct single shooting

This method solves the OCP by discretizing the optimal control as piecewise constant signals over the entire interval, with the states as dependent variables by forward integration. This can be likened to experimentally guessing a proper input and watching the result, repeating until optimality is reached [18]. The general computation load is relatively low because the control is the only NLP decision variable. These methods do not handle complicated systems well however.

2.4.0.2 Direct multiple shooting

The control input discretization is done as in direct single shooting but over a series of shorter intervals. It also solves the ODEs separately to obtain the states at shooting nodes as additional decision variables [17]. This can secure continuity of the state trajectories at the expense of a much larger NLP. Complicated systems are handled better than by direct single shooting [18].

2.4.0.3 Direct collocation

This method uses collocation to enforce system dynamics and constraints on a set of points in each sub-interval known as collocation points [17]. The controls may be discretized as piecewise constant or piecewise polynomial. The approximations of the state trajectories may be more accurate compared to direct single shooting and direct multiple shooting. Computation time may be faster than that of direct multiple shooting, and has been used for solving optimal control problems with success [19].

2.4.1 CasADi

CasADi is one of numerous open-source optimization tools for solving general optimization problems and optimal control problems [20]. CasADi can be used with MATLAB, where the optimization variables, constraints and objective function handily are defined symbolically. CasADi is well suited to handle even complex non-linear model predictive problems in MATLAB [21].

2.4.2 Model predictive control

The previous OCP methods have so far only considered total horizon or open-loop control. Typically a more real-time based approach will provide more satisfying results compared to a real system. The OCP methods can be used to drive a model predictive control strategy, which has been done in a solar energy thermal system as an example [22].

Model predictive control (MPC) is an advanced control engineering method that was first used in the process industry in the 1980s that concerns complex models of MIMO (multi-input multi-output) systems. The main goal of the control algorithm is to simulate the system model forward for a certain amount of time called the horizon. The horizon is split into a specific number of control points that determines

the resolution of the simulations. The model predictive controller calculates optimal control inputs over the horizon while simultaneously considering the system states. The first element of the optimal control signal sequence is then applied to the system. By repeating this process every sample, a so called receding horizon controller has been implemented [23]. The method is called receding horizon control because the horizon effectively moves forward in time for each iteration while continuously optimizing inputs based on changing conditions.

The optimal control involves minimizing or maximizing a cost function that may consist of several terms, such as the states of the system, inputs and disturbances. The optimization problem is subject to constraints that represent physical limitations or forbidden actions that must be fulfilled over the entire horizon.

The advantages of receding horizon control are numerous, such as increased performance, enforcing constraints and improved robustness compared to more basic control methods. Disadvantages involve the need for a detailed model, which means higher initial costs of implementation. The system model may also degrade over time, and may make troubleshooting trickier. Stability of a receding horizon controller can be hard to guarantee, yet it is possible [24]. The property of anticipating and mitigating future disturbances is of great interest for our thermal system.

The performance of model predictive controllers can be evaluated and tuned in several ways. The horizon length and number of control inputs can be increased to improve detail and incorporate more of future dynamics, often at the expense of much longer computation time. The cost function weights can be changed to promote desired behavior.

2.4.2.1 Nonlinear model predictive control

The difference between "regular" and nonlinear model predictive control (NMPC) lays in the underlying system dynamics. Regular MPC is based on linear system dynamics while NMPC deals with nonlinear system dynamics. NMPC can be utilized for problems such as energy optimal nonlinear vehicle cruise control [25]. It is also possible to simplify an NMPC by linearization [26].

3
Methods

3.1 Physical modelling

The notations used in the chapter are expressed in the Nomenclature. Coolant temperature relations where the dynamic coupling will be expressed, utilizing heats and mixing relations. Several assumptions are made: one-dimensional heat transfer, the fluid properties are constant, no phase change, negligible kinetic and potential energy, no heat loss through the pipes and ideal mixing. The valve decoupling position η_d indicates the flow configuration of the system. The system is decoupled when $\eta_d = 0$, coupled when $\eta_d = 1$ and a mix of the two for $0 < \eta_d < 1$.

Applying a heat balance over the first temperature T_1 with the assumptions stated, simplifying and solving for T_1 gives

$$T_1 = \eta_d T_4 + (1 - \eta_d) T_3, \tag{3.1}$$

meaning that $T_1 = T_3$ when $\eta_d = 0$ and $T_1 = T_4$ when $\eta_d = 1$. Between the positions of T_1 and T_2, the heater/chiller unit supplies external heating or cooling. An energy balance is made and simplified which gives the expression

$$T_2 = T_1 + \frac{\dot{Q}_{ch}}{\rho_c f_B C_{p,c}}. \tag{3.2}$$

The energy balance procedure is repeated for the rest of the coolant temperatures which gives the expressions

$$\begin{aligned} T_3 &= T_2 + \frac{\dot{Q}_{cB}}{\rho_c f_B C_{p,c}}, \\ T_4 &= \eta_r T_7 + (1 - \eta_r) T_6, \\ T_5 &= \eta_d T_3 + (1 - \eta_d) T_4, \\ T_6 &= T_5 + \frac{\dot{Q}_{cM}}{\rho_c f_M C_{p,c}}, \\ T_7 &= T_6 + \frac{\dot{Q}_r}{\rho_c f_M C_{p,c}}. \end{aligned} \tag{3.3}$$

3.1.0.1 ESS heat transfer

A heat balance over the electric storage system, shortened to B for battery, gives

$$m_B C_{p,B} \dot{T}_B = \dot{Q}_{ESS} - \dot{Q}_{cB} - \dot{Q}^B_{env}, \tag{3.4}$$

where the individual heat transfer rates are defined as

$$\begin{aligned}\dot{Q}^B_{env} &= \alpha^B_{env}(T_B - T_{amb})\\ \dot{Q}_{ESS} &= RI^2\end{aligned}$$

The rate of heat transfer between the battery and coolant $\dot{Q}_{cB}$ will be modeled as a heat exchanger using the Number of Transfer Units (NTU) method assuming the coolant is the only stream (c.f. Equation 2.16).

$$\begin{aligned}\dot{Q}_{cB} &= \epsilon_B C_{min,B}(T_B - T_2)\\ &= \epsilon_B C_{min,B}(T_B - (T_1 + \frac{\dot{Q}_{ch}}{C_{min,B}}))\end{aligned} \tag{3.5}$$

where the heater/chiller unit satisfies

$$\dot{Q}^{min}_{ch} \leq \dot{Q}_{ch} \leq \dot{Q}^{max}_{ch}, \tag{3.6}$$

and is regarded as an input, which can deliver a given heating or cooling power.

The overall heat transfer coefficient U_B for the ESS is assumed to be equal to the convective heat transfer coefficient h_B of the coolant and is derived from the dimensionless Prandtl, Reynold and Nusselt numbers. Turbulent flow is known to be occurring for the relevant system configurations and is therefore used for the Nusselt relation.

$$\begin{aligned}v &= \frac{4f}{\pi D^2},\\ Re &= \frac{\rho_c v D}{\mu_c},\\ Pr &= \frac{\mu_c C_p}{k},\\ Nu &= 0.023 Re^{0.8} Pr^{0.35},\\ h_B &= \frac{Nu \cdot k_c}{D}.\end{aligned} \tag{3.7}$$

The overall heat transfer coefficient is then assumed to be limited by the convective heat transfer coefficient:

$$\frac{1}{U_B} = \frac{1}{h_B}. \tag{3.8}$$

The NTU, the *number of transfer units*, equals

$$NTU = \frac{U_B A}{C_{min}}, \tag{3.9}$$

where

$$C_{min} = \rho_c f C_p. \tag{3.10}$$

Because of the assumption that the coolant is the only stream exchanging heat, the relation for ϵ_B becomes

$$\epsilon_B = 1 - e^{-NTU}. \tag{3.11}$$

3.1.0.2 MDS heat transfer

The heat balance over the motor drive system, shortened to M for motor, is similar to the battery;

$$m_M C_{p,M} \dot{T}_M = \dot{Q}_{MDS} - \dot{Q}_{cM} - \dot{Q}^M_{env} \tag{3.12}$$

The heat dissipation to the environment and heat generation by the MDS are also similar:

$$\begin{aligned} \dot{Q}^M_{env} &= \alpha^M_{env}(T_{amb} - T_M), \\ \dot{Q}_{MDS} &= \alpha_H P_M, \end{aligned}$$

where α_H is a coefficient relating the power demand P_M to the amount of heat generated. Determining the actual value of this coefficient is outside the scope at this time and it is therefore assigned an estimate. The heat transferred to the coolant is modelled in a very similar way as for the ESS. The derivation of the effectiveness parameter ϵ_M is therefore spared:

$$\dot{Q}_{cM} = \epsilon_M C_{min,M}(T_M - T_5). \tag{3.13}$$

3.1.0.3 Radiator heat transfer

The heat removed by the radiator is modelled with by convective heat transfer relations for the external and internal heat transfer. The internal convective heat transfer, the heat concerning the coolant fluid, is modelled similarly to $\dot{Q}_{cB}$ and $\dot{Q}_{cM}$. The internal convective heat transfer coefficient h_i is calculated as:

$$\begin{aligned} v &= \frac{4 f_M}{\pi D^2} \\ Re &= \frac{\rho_c v D}{\mu_c} \\ Pr &= \frac{\mu_c C_{p,c}}{k_c} \end{aligned} \tag{3.14}$$

$$Nu = 0.023 Re^{0.8} Pr^{0.35} \tag{3.15}$$

$$h_i = \frac{Nu \cdot k_c}{D} \tag{3.16}$$

The heat to the surrounding air will be modeled by relations for forced convection for external flow [10]. The air velocity is approximated using the following relation:

$$v_{air} = v_v + \left(1 - \frac{v_v}{v_{v,max}}\right)\beta_f \omega_f, \tag{3.17}$$

where the vehicle speed v_v contributes to the air speed by ram-air (the air that enters the vehicle due to the vehicle speed) intake. The air speed contribution of the fan is modeled as a coefficient β_f times the fan angular speed ω_f. The quotient in the

second term takes into an approximate account to the reduced fan effectiveness as vehicle speed increases. The Prandtl and Reynolds numbers are

$$\begin{aligned} Pr &= \frac{\mu_{air} C_{p,air}}{k_{air}}, \\ Re &= \frac{\rho_{air} v_{air} L_r}{\mu_{air}}, \end{aligned} \tag{3.18}$$

where L_r is some assumed characteristic length of the radiator. The correlation for the Nusselt number in this heat transfer case utilizes Equation 19-36 in [10], which assumes turbulent flow:

$$Nu = 0.3 + \frac{0.62 Re^{1/2} Pr^{1/3}}{[1 + (0.4/Pr)^{2/3}]^{1/4}} \left[1 + \left(\frac{Re}{282000} \right)^{5/8} \right]^{4/5} \tag{3.19}$$

This leads to an expression for the outer convective heat transfer coefficient,

$$h_o = \frac{Nu \cdot k_{air}}{L_r} \tag{3.20}$$

An expression for the overall heat transfer coefficient U for the radiator can now be made where the conductive heat transfer resistance is assumed to be negligible.

$$\frac{1}{U} = \frac{1}{h_i} + \frac{1}{h_o} \tag{3.21}$$

The NTU method is now ready to be applied. The heat capacity rates of the flows are calculated as

$$\begin{aligned} C_c &= \rho_c f_M C_{p,c}, \\ C_{air} &= \rho_{air} A_{air} v_{air} C_{p,air}, \end{aligned} \tag{3.22}$$

where A_{air} is an assumed area for radiator area facing the vehicle front. The heat capacity ratio is defined as:

$$C_r = \frac{C_c}{C_{air}}. \tag{3.23}$$

The lesser of the two heat capacity rates C_{air} and C_c was from testing concluded for most operations to be the one of the coolant i.e. $C_{min} = C_c$. The NTU becomes then

$$NTU = \frac{U A_r}{C_c}, \tag{3.24}$$

where A_r is an assumed heat transfer area in the radiator. The efficiency parameter is then calculated from a relation assuming a single-pass cross-flow configuration in [9]:

$$\epsilon_r = 1 - exp\left(\frac{1}{C_r} NTU^{0.22} \Big(exp(-C_r NTU^{0.78}) - 1 \Big) \right). \tag{3.25}$$

The expression for the radiator heat transfer can now be stated as

$$\begin{aligned} \dot{Q}_r &= \epsilon_r C_c (T_{amb} - T_6) \\ &= \epsilon_r C_c \left(T_{amb} - (T_5 + \frac{\dot{Q}_{cM}}{\rho_c f_M C_{p,c}}) \right). \end{aligned} \tag{3.26}$$

3.1.0.4 Coolant temperature modelling

The amount of coolant temperatures needed to encapsule the dynamics can be reduced to two. The potential and mechanical energies are assumed to be negligible for the heat transfer problem, leaving only thermal energies. Heat balances over adiabatic control volumes for T_1 and T_5 can be made by utilizing the first law of thermodynamics, assuming no heat generation inside ($\dot{E}_{gen} = 0$), i.e.

$$\frac{\partial E}{\partial t} = \dot{E}_{in} - \dot{E}_{out}. \tag{3.27}$$

Perfect mixing is assumed, leading to no temperature gradient in the control volume. For T_1 a relation for the decoupled mode is made, followed by another for coupled mode. Starting with decoupled mode (i.e. $\eta_d = 0$);

$$\frac{\partial}{\partial t}(\rho_c V_1 C_{p,c} T_1) = \rho_c f_B C_{p,c} T_3 - \rho_c f_B C_{p,c} T_1, \tag{3.28}$$

which, given constant density, specific heat and volume gives

$$\dot{T}_1 = \frac{f_B}{V_1}(T_3 - T_1). \tag{3.29}$$

The above relation can be made dependent on T_1 and T_5 by substituting for T_3 several times with the expressions in (3.3).

$$\begin{aligned} T_3 &= T_2 + \frac{\dot{Q}_{cB}}{\rho_c f_B C_{p,c}} \\ &= T_1 + \frac{\dot{Q}_{ch}}{\rho_c f_B C_{p,c}} + \frac{\dot{Q}_{cB}}{\rho_c f_B C_{p,c}}, \end{aligned} \tag{3.30}$$

Substituting this back to Equation 3.28 we get the final decoupled relation for $\dot{T}_1$:

$$\begin{aligned} \dot{T}_1 &= \frac{f_B}{V_1}(\cancel{T_1} + \frac{\dot{Q}_{ch}}{\rho_c f_B C_{p,c}} + \frac{\dot{Q}_{cB}}{\rho_c f_B C_{p,c}} - \cancel{T_1}) \\ &= \frac{\dot{Q}_{ch} + \dot{Q}_{cB}}{\rho_c V_1 C_{p,c}} \end{aligned} \tag{3.31}$$

The coupled relation is derived in a similar fashion. However the volumetric flow considered for the coupled case is still the one of the battery. The two flows will in fully coupled mode become one according to the following equality constraint;

$$f_M = f_M + \eta_d(f_B - f_M) \tag{3.32}$$

Meaning that $\eta_d = 0 \implies f_M = f_M$ and $\eta_d = 1 \implies f_M = f_B$. This implies

$$\begin{aligned} \frac{\partial}{\partial t}(\rho_c V_1 C_{p,c} T_1) &= \rho_c f_B C_{p,c} T_4 - \rho_c f_B C_{p,c} T_1, \\ \dot{T}_1 &= \frac{f_B}{V_1}(T_4 - T_1). \end{aligned} \tag{3.33}$$

This time the relation can again be made dependent on T_5 and T_1 by substituting by T_4.

$$\begin{aligned}
T_4 &= \eta_r T_7 + (1-\eta_r)T_6 \\
&= \eta_r(T_6 + \frac{\dot{Q}_r}{\rho_c f_M C_{p,c}}) + (1-\eta_r)T_6 \\
&= \eta_r(T_5 + \frac{\dot{Q}_{cM}}{\rho_c f_M C_{p,c}} + \frac{\dot{Q}_r}{\rho_c f_M C_{p,c}}) + (1-\eta_r)(T_5 + \frac{\dot{Q}_{cM}}{\rho_c f_M C_{p,c}}) \\
&= \cancel{\eta_r T_5} + \cancel{\eta_r \frac{\dot{Q}_{cM}}{\rho_c f_M C_{p,c}}} + \eta_r \frac{\dot{Q}_f}{\rho_c f_M C_{p,c}} + T_5 + \frac{\dot{Q}_{cM}}{\rho_c f_M C_{p,c}} - \cancel{\eta_r T_5} - \cancel{\eta_r \frac{\dot{Q}_{cM}}{\rho_c f_M C_{p,c}}} \\
&= T_5 + \frac{\dot{Q}_{cM} + \eta_r \dot{Q}_r}{\rho_c f_M C_{p,c}}
\end{aligned} \tag{3.34}$$

The final expression for T_1 in the coupled case becomes;

$$\begin{aligned}
\dot{T}_1 &= \frac{f_B}{V_1}(T_4 - T_1) \\
\dot{T}_1 &= \frac{f_B}{V_1}((T_5 + \frac{\dot{Q}_{cM} + \eta_r \dot{Q}_r}{\cancel{\rho_c f_M C_{p,c}}}) - T_1) \qquad \eta_d = 1 \Rightarrow f_M = f_B \\
\dot{T}_1 &= \frac{1}{V_1}(f_B(T_5 - T_1) + \frac{\dot{Q}_{cM} + \eta_r \dot{Q}_r}{\rho_c C_{p,c}})
\end{aligned} \tag{3.35}$$

The decoupled and coupled expressions are then joined together to get

$$\dot{T}_1 = \eta_d \left(\frac{1}{V_1}(f_B(T_5 - T_1) + \frac{\dot{Q}_{cM} + \eta_r \dot{Q}_r}{\rho_c C_{p,c}}) \right) + (1-\eta_d)\left(\frac{\dot{Q}_{ch} + \dot{Q}_{cB}}{\rho_c V_1 C_{p,c}} \right) \tag{3.36}$$

Now, from T_1 we now have T_3 from Equation 3.30 and T_2 from Equation 3.2. The procedure is repeated for T_5, starting with decoupled mode:

$$\begin{aligned}
\frac{\partial}{\partial t}(\rho_c V_5 C_{p,c} T_5) &= \rho_c f_M C_{p,c} T_4 - \rho_c f_M C_{p,c} T_5 \\
\dot{T}_5 &= \frac{f_M}{V_5}(T_4 - T_5)
\end{aligned} \tag{3.37}$$

Substituting directly with the expression for T_4 derived in Equation 3.34 we get

$$\begin{aligned}
\dot{T}_5 &= \frac{f_M}{V_5}(\cancel{T_5} + \frac{\dot{Q}_{cM} + \eta_r \dot{Q}_r}{\rho_c f_M C_{p,c}} - \cancel{T_5}) \\
&= \frac{\cancel{f_M}}{V_5}(\frac{\dot{Q}_{cM} + \eta_r \dot{Q}_r}{\rho_c \cancel{f_M} C_{p,c}}) \\
&= \frac{\dot{Q}_{cM} + \eta_r \dot{Q}_r}{\rho_c V_5 C_{p,c}}
\end{aligned} \tag{3.38}$$

As before, the expression for the coupled mode is made. The volumetric flow considered for the coupled mode is as before the greater of the two, the battery flow;

$$\begin{aligned}\frac{\partial}{\partial t}(\rho_c V_5 C_{p,c} T_5) &= \rho_c f_B C_{p,c} T_3 - \rho_c f_B C_{p,c} T_5 \\ \dot{T}_5 &= \frac{f_B}{V_5}(T_3 - T_5)\end{aligned} \tag{3.39}$$

Inserting the expression for T_3, in Equation 3.30, gives

$$\begin{aligned}\dot{T}_5 &= \frac{f_B}{V_5}((T_1 + \frac{\dot{Q}_{ch}}{\rho_c f_B C_{p,c}} + \frac{\dot{Q}_{cB}}{\rho_c f_B C_{p,c}}) - T_5) \\ &= \frac{1}{V_5}(f_B(T_1 - T_5) + \cancel{f_B}\frac{\dot{Q}_{ch} + \dot{Q}_{cB}}{\rho_c \cancel{f_B} C_{p,c}})) \\ &= \frac{1}{V_5}(f_B(T_1 - T_5) + \frac{\dot{Q}_{ch} + \dot{Q}_{cB}}{\rho_c C_{p,c}}))\end{aligned} \tag{3.40}$$

The decoupled and coupled modes for $\dot{T}_5$ are as before joined into one expression:

$$\dot{T}_5 = \eta_d\left(\frac{1}{V_5}(f_B(T_1 - T_5) + \frac{\dot{Q}_{ch} + \dot{Q}_{cB}}{\rho_c C_{p,c}})\right) + (1 - \eta_d)\left(\frac{\dot{Q}_{cM} + \eta_r \dot{Q}_r}{\rho_c V_5 C_{p,c}}\right) \tag{3.41}$$

Now, since T_6 is given by T_5, and T_7 by T_6 according to (3.3), only the coolant temperatures T_1 and T_5 need to be included in a state-space model. It is now possible to place the ESS, MDS and two coolant temperatures on a state-space form.

$$\dot{T}_B = \frac{1}{m_B C_{p,B}}(\dot{Q}_{ESS} - \dot{Q}_{cB} - \dot{Q}^B_{env}) \tag{3.42}$$

$$\dot{T}_M = \frac{1}{m_M C_{p,M}}(\dot{Q}_{MDS} - \dot{Q}_{cM} - \dot{Q}^M_{env}) \tag{3.43}$$

$$\dot{T}_1 = \eta_d\left(\frac{1}{V_1}(f_B(T_5 - T_1) + \frac{\dot{Q}_{cM} + \eta_r \dot{Q}_r}{\rho_c C_{p,c}})\right) + (1 - \eta_d)\left(\frac{\dot{Q}_{ch} + \dot{Q}_{cB}}{\rho_c V_1 C_{p,c}}\right) \tag{3.44}$$

$$\dot{T}_5 = \eta_d\left(\frac{1}{V_5}(f_B(T_1 - T_5) + \frac{\dot{Q}_{ch} + \dot{Q}_{cB}}{\rho_c C_{p,c}})\right) + (1 - \eta_d)\left(\frac{\dot{Q}_{cM} + \eta_r \dot{Q}_r}{\rho_c V_5 C_{p,c}}\right) \tag{3.45}$$

The system can now be rewritten in general nonlinear state-space form

$$\dot{x} = f(x, u) + d, \tag{3.46}$$

where

$$f(x, u) = [\dot{T}_B \quad \dot{T}_M \quad \dot{T}_1 \quad \dot{T}_5]^T, \tag{3.47}$$

$$x = [T_B \quad T_M \quad T_1 \quad T_5]^T, \quad u = [\dot{Q}_{ch} \quad \omega_f \quad f_B \quad f_M \quad \eta_d \quad \eta_r]^T \tag{3.48}$$

$$d = [\dot{Q}_{ESS} \quad \dot{Q}_{MDS} \quad T_{amb} \quad v_v]^T, \tag{3.49}$$

where

$$f(x,u) = \begin{bmatrix} \frac{1}{m_B C_{p,B}}\Big(\epsilon_B C_B\big((x_3 + \frac{u_1}{\rho_c u_3 C_{p,f}}) - x_1\big) + d_1 + \alpha^B_{env}\big(d_3 - x_1\big)\Big) \\ \frac{1}{m_M C_{p,M}}\Big(\epsilon_M C_M\big(x_4 - x_2\big) + d_2 + \alpha^M_{env}\big(d_3 - x_2\big)\Big) \\ u_5 \frac{1}{V_1}\Big(u_3(x_4 - x_3) + \frac{\epsilon_M C_M\big(x_2 - x_4\big) + u_6\dot{Q}_r}{\rho_c C_{p,c}}\Big) + \Big(1 - u_5\Big)\Big(\frac{u_1 + \epsilon_B C_B\big(x_1 - (x_3 + \frac{u_1}{\rho_c u_3 C_{p,f}})\big)}{\rho_c V_1 C_{p,c}}\Big) \\ u_5 \frac{1}{V_5}\Big(u_3(x_3 - x_4) + \frac{\epsilon_B C_B\big(x_1 - (x_3 + \frac{u_1}{\rho_c u_3 C_{p,f}})\big) + u_1}{\rho_c C_{p,c}}\Big) + \Big(1 - u_5\Big)\Big(\frac{\epsilon_M C_M\big(x_2 - x_4\big) + u_6\dot{Q}_r}{\rho_c V_5 C_{p,c}}\Big) \end{bmatrix}. \tag{3.50}$$

3.2 Stability & controllability analysis

Analyzing stability of linear systems is significantly more straight forward than for nonlinear systems. The nonlinear properties can be roughly approximated by its linear approximation. The dynamics were therefore put on matrix form and the resulting jacobian system matrix A and input matrix B were derived by linearization for stability analysis at certain probable operating points. The explicit linearized matrices can be found in the appendix.

3.2.1 First operating point, fully decoupled ($\eta_d = 0$)

The first operating point assumes the battery and motor drive system values at their respective reference values, no heating or cooling, battery coolant flow rate at 7 liters per minute, motor drive system coolant flow rate at 10 liters per minute, no battery or motor drive system power demands and an ambient temperature at zero degrees Celsius:

$$\begin{aligned} x_{op1} &= [22.5 \quad 100 \quad 22.5 \quad 100]^T \\ u_{op1} &= [0 \quad 0 \quad \frac{7}{60000} \quad \frac{42}{60000} \quad 0 \quad 0]^T \\ d_{op1} &= [1000 \quad 350 \quad 40]^T \end{aligned} \tag{3.51}$$

The matrices with numerical values are spared from the report, but the eigenvalue vector is included as

$$\lambda_{op1} = \begin{bmatrix} -8.427 \cdot 10^{-6} \\ -0.00331 \\ -1.820 \cdot 10^{-5} \\ -0.00228 \end{bmatrix} \tag{3.52}$$

Assuming continuous dynamics for now, the eigenvalues indicate that the linearized system is stable at the operating point because the values are located in the left half-plane. The eigenvalues differ substantially in magnitude, which indicates that the system is stiff. There is no exact satisfactory definition of stiffness, but a good estimate can be made with the following *stiffness ratio*:

$$\frac{|(Re(\overline{\lambda})|}{|(Re(\underline{\lambda})|}, \tag{3.53}$$

i.e. dividing the largest absolute real valued eigenvalue by the lowest absolute real valued eigenvalue, which in this case results in

$$\frac{|(Re(\overline{\lambda}_{op1})|}{|(Re(\underline{\lambda}_{op1})|} = \frac{0.00331}{8.427 \cdot 10^{-6}} \approx 393, \tag{3.54}$$

which is somewhat large. The combination of negative eigenvalue and a moderate stiffness ratio characterizes the system as stiff. This indicates that caution has to be made when simulating the system, using appropriately small time steps to avoid numerical instability.

Another property of the system that is relevant to determine is its controllability, which can be done be utilizing the system and input matrices. A linear system consisting of a $n \times n$ system matrix A and $n \times r$ input matrix B is controllable if the $n \times nr$ controllability matrix

$$S = [B \quad AB \quad A^2B \quad ... \quad A^{n-1}B], \tag{3.55}$$

has full rank, i.e. $rank(S) = n$. The resulting 4×24 controllability matrix is spared from being explicitly stated in this report but was found to have full rank ($rank(S_{op1}) = 4 = n$), meaning the system is controllable for the operating point.

3.2.2 Second operating point, fully coupled ($\eta_d = 1$)

From preliminary simulation results, the valve decoupling input signal changes the temperatures at a faster rate than any other. Therefore the next operating point will consider the case of full coupling $\eta_d = 1$. This would bring the coolant temperatures to converge as they effectively become one coolant system and is reflected in the new operating point. The flow rate values also combine into one, the other values are the same as in the first operating point.

$$\begin{aligned} x_{op2} &= [22.5 \quad 100 \quad 60 \quad 60]^T \\ u_{op2} &= [0 \quad 0 \quad \frac{42}{60000} \quad \frac{42}{60000} \quad 1 \quad 0]^T \\ d_{op2} &= [1000 \quad 350 \quad 40]^T \end{aligned} \tag{3.56}$$

The eigenvalues at this operating point are

$$\lambda_{op2} = \begin{bmatrix} -0.003643 \\ -0.004601 \\ -3.151 \cdot 10^{-6} \\ -1.718 \cdot 10^{-4} \end{bmatrix} \tag{3.57}$$

The magnitude of the eigenvalues are similar to the first operating point in Equation 3.52. Fortunately, the eigenvalues are again all negative indicating stability even if the system is fully coupled! A new stiffness ratio is calculated:

$$\frac{|(Re(\overline{\lambda}_{op2})|}{|(Re(\underline{\lambda}_{op2})|} = \frac{0.02282}{1.814 \cdot 10^{-6}} \approx 1460. \tag{3.58}$$

The stiffness ratio is significantly larger than in the first case. Controllability is interesting also for this operating point. The rank of the controllability matrix was found to be

$$rank(S_{op2}) = 4 = n, \tag{3.59}$$

which means that this operating point is also controllable. An approximation of the nonlinear properties can be derived from these two crucial linearized operating points. The nonlinear system is therefore assumed to be stable and controllable, but very stiff. **Important note!** This approximate assumption does not prove that the original nonlinear system is stable nor that is is always controllable!

3.3 Optimization formulation

The nonlinear control task can be formulated as nonlinear optimization problem for use in the upcoming receding horizon control strategy.

$$\begin{aligned} \min \quad & \sum_{0}^{N-1} \Big(w_1 u_1^2 + w_2 u_2^2 + w_3 u_3^2 + w_4 u_4^2 + w_5 (x_1 - r_1)^2 + w_6 (x_2 - r_2)^2 \Big) \\ & + w_7 (x_1(N) - r_1)^2 + w_8 (x_2(N) - r_2)^2 \end{aligned}$$

$$\begin{aligned} \text{subject to} \quad & -6000 \leq u_1 \leq 9000, && [W], \\ & 0 \leq u_2 \leq 600, && [RPM], \\ & 42 \leq u_3 \leq 60, && [l/min], \\ & 7 \leq u_4 \leq 12, && [l/min], \\ & 0 \leq u_5 \leq 1, && [*] \\ & 0 \leq u_6 \leq 1, && [*] \\ & 16.5 \leq x_1 \leq 28.5, && [^\circ C] \\ & 75 \leq x_2 \leq 125, && [^\circ C] \\ & -35 \leq x_3 \leq 106, && [^\circ C] \\ & -35 \leq x_4 \leq 106, && [^\circ C] \end{aligned} \tag{3.60}$$

$$\dot{x}_1 = \frac{1}{m_B C_{p,B}}\Big(\epsilon_B C_B((x_3 + \frac{u_1}{\rho_c u_3 C_{p,f}}) - x_1) + d_1 + \alpha^B_{env}(d_3 - x_1)\Big)$$
$$\dot{x}_2 = \frac{1}{m_M C_{p,M}}\Big(\epsilon_M C_M(x_4 - x_2) + d_2 + \alpha^M_{env}(d_3 - x_2)\Big)$$
$$\dot{x}_3 = \Bigg[u_5 \frac{1}{V_1}\Big(u_3(x_4 - x_3) + \frac{\epsilon_M C_M(x_2 - x_4) + u_6\dot{Q}_r}{\rho_c C_{p,c}}\Big) + \Big(1 - u_5\Big)\Big(\frac{u_1 + \epsilon_B C_B(x_1 - (x_3 + \frac{u_1}{\rho_c u_3 C_{p,f}}))}{\rho_c V_1 C_{p,c}}\Big)\Bigg]$$
$$\dot{x}_4 = \Bigg[u_5 \frac{1}{V_5}\Big(u_3(x_3 - x_4) + \frac{\epsilon_B C_B(x_1 - (x_3 + \frac{u_1}{\rho_c u_3 C_{p,f}})) + u_1}{\rho_c C_{p,c}}\Big) + \Big(1 - u_5\Big)\Big(\frac{\epsilon_M C_M(x_2 - x_4) + u_6\dot{Q}_r}{\rho_c V_5 C_{p,c}}\Big)\Bigg]$$
$$u_4 = u_4 + u_5(u_3 - u_4)$$
$$\dot{Q}_r = \epsilon_r C_c\Big(d_3 - (x_4 + \frac{\epsilon_M C_M(x_4 - x_2)}{\rho_c u_4 C_{p,c}}\Big)$$

The model can be rewritten in terms of vectors of state variables, input variables, references and disturbances to give a more general formulation. The vectors are to be used as components for the objective function, inequality constraint matrix and equality constraint matrix.

$$l = w_1 u_1^2 + w_2 u_2^2 + w_3 u_3^2 + w_4 u_4^2 + w_5(x_1 - r_1)^2 + w_6(x_2 - r_2)^2 \tag{3.61}$$

$$b = \begin{bmatrix} \underline{x_1} & \overline{x_1} & \underline{x_2} & \overline{x_2} & \underline{x_3} & \overline{x_3} & \underline{x_4} & \overline{x_4} & \underline{u_1} & \overline{u_1} & \underline{u_2} & \overline{u_2} & \underline{u_3} & \overline{u_3} & \underline{u_4} & \overline{u_4} \end{bmatrix} \tag{3.62}$$

The inequality matrix g houses both the lower and upper bound inequalities of the problem.

$$g = \begin{bmatrix} b_1 - x_1 \\ x_1 - b_2 \\ b_3 - x_2 \\ x_2 - b_4 \\ b_5 - x_3 \\ x_3 - b_6 \\ b_7 - x_4 \\ x_4 - b_8 \\ b_9 - u_1 \\ u_1 - b_{10} \\ b_{11} - u_2 \\ u_2 - b_{12} \\ b_{13} - u_3 \\ u_3 - b_{14} \\ b_{15} - u_4 \\ u_4 - b_{16} \\ -u_5 \\ u_5 - 1 \\ -u_6 \\ u_6 - 1 \end{bmatrix} \tag{3.63}$$

The equality vector h puts the system dynamics into state constraints.

$$h = \begin{bmatrix} -\dot{x}_1 + \frac{1}{m_B C_{p,B}}\Big(\epsilon_B C_B\big((x_3 + \frac{u_1}{\rho_c u_3 C_{p,f}}) - x_1\big) + d_1 + \alpha^B_{env}\big(d_3 - x_1\big)\Big) \\ -\dot{x}_2 + \frac{1}{m_M C_{p,M}}\Big(\epsilon_M C_M\big(x_4 - x_2\big) + d_2 + \alpha^M_{env}\big(d_3 - x_2\big)\Big) \\ -\dot{x}_3 + \Bigg[u_5 \frac{1}{V_1}\Bigg(u_3(x_4 - x_3) + \frac{\epsilon_M C_M\big(x_2 - x_4\big) + u_6\dot{Q}_r}{\rho_c C_{p,c}}\Bigg) + \Big(1 - u_5\Big)\Bigg(\frac{u_1 + \epsilon_B C_B\big(x_1 - (x_3 + \frac{u_1}{\rho_c u_3 C_{p,f}})\big)}{\rho_c V_1 C_{p,c}}\Bigg)\Bigg] \\ -\dot{x}_4 + \Bigg[u_5 \frac{1}{V_5}\Bigg(u_3(x_3 - x_4) + \frac{\epsilon_B C_B\big(x_1 - (x_3 + \frac{u_1}{\rho_c u_3 C_{p,f}})\big) + u_1}{\rho_c C_{p,c}}\Bigg) + \Big(1 - u_5\Big)\Bigg(\frac{\epsilon_M C_M\big(x_2 - x_4\big) + u_6\dot{Q}_r}{\rho_c V_5 C_{p,c}}\Bigg)\Bigg] \\ -u_4 + u_4(0) + u_5(u_3 - u_4(0)) \\ -\dot{Q}_r + \epsilon_r C_M\Bigg(d_3 - \big(x_4 + (\epsilon_M C_M \frac{x_2 - x_4}{\rho_c u_4 C_{p,c}})\big)\Bigg) \end{bmatrix} \tag{3.64}$$

These functions make way for a general NLP formulation.

$$\begin{aligned} \min_{x,u} \quad & l(x,u) \\ s.t. \quad & g(x,u) \leq 0 \\ & h(x,u) = 0 \end{aligned} \tag{3.65}$$

3.3.1 Solving the optimization problem

To aid the nonlinear solver *direct collocation* is used [17]. The time horizon T of the infinite optimal control problem is discretized on a set of N points, giving time step length $dh = T/N$. System dynamics are enforced at each boundary condition of the time points and are sometimes denoted as helper states $x^c_k(t_k) \approx x_k(t_k)$. The control signals are parameterized on the same time grid as piecewise constants $u_k(t_k)$.
In each collocation interval $[t_k, t_{k+1}]$ there is a set of collocation points $\tau^1_k, ..., \tau^d_k$, which are defined by Legendre polynomials $p_k(t_k, v_k(\tau))$ of degree d (1 to 3), where $v_k(\tau)$ is the coefficient vector dependent on the degree. This degree can be chosen at will depending on the desired optimization performance. The system trajectory is approximated using these polynomials. The general expression for the first three degrees of Legendre polynomials on the interval $[0, 1]$ are:

$$\begin{aligned} P_1(x) &= 2x - 1 \\ P_2(x) &= 6x^2 - 6x + 1 \\ P_3(x) &= 20x^3 - 30x^2 + 12x - 1 \end{aligned} \tag{3.66}$$

The number of collocation points τ in each interval should equal the degree of the polynomial, and their relative positions equal the zeros of the Legendre polynomials.

$$\begin{aligned} \tau_{d=1} &= [0.5] \\ \tau_{d=2} &\approx [0.211,\ 0.789] \\ \tau_{d=3} &\approx [0.113,\ 0.500,\ 0.887] \end{aligned} \tag{3.67}$$

The coefficient vector $v_k(\tau)$ is defined using these values. The Legendre polynomials together with their zeros can be seen in Figure 3.1.

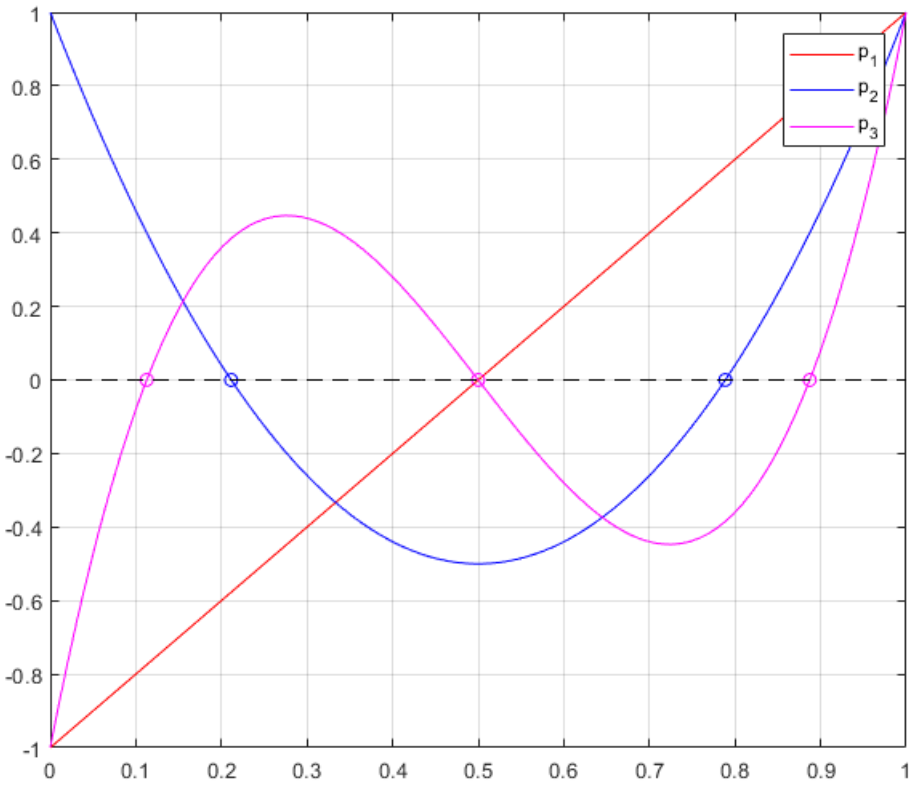

Figure 3.1: Legendre polynomials on the interval $[0, 1]$ of degrees 1, 2 and 3. The circles indicate the zeros of the polynomials.

The system dynamics and objective function are defined in the function f,

$$[x_c(k+1), q(k)] = f(x_c(k), u(k)) \tag{3.68}$$

The equality constraints of the optimization problem then becomes:

$$\begin{aligned} x_c(k) - p_k(t_k, v_k) &= 0 \\ f(p_k(t_k^1, v_k), u_k(t_k^1)) - \dot{p}_k(t_k^1, v) &= 0 \\ &\vdots \\ f(p_k(t_k^d, v_k), u_k(t_k^1)) - \dot{p}_k(t_k^d, v) &= 0 \end{aligned} \tag{3.69}$$

The equality terms are combined into a collocation condition vector

$$c_k(x_c(k), v_k) = 0, \tag{3.70}$$

and continuity conditions are stated on the form:

$$x_c(k+1) = p_k(t_k, v_k)dh \tag{3.71}$$

The objective function is approximated using a quadrature formula

$$l(k+1) = l(k) + q(k)v_k dh, \tag{3.72}$$

which arrives at the final optimization formulation for the direct collocation, which is a large but likewise sparse nonlinear programming problem:

$$\begin{aligned}
&\min_{x_c,v,u} && \sum_{k=0}^{N-1} l_k(x_c(k), v_k, u(k)) \\
&\textit{subject to} \\
&x_c(0) - x_0 = 0, && && \text{(initial conditions)} \\
&c_k(x_c(k), v_k) = 0, && k = 0, \ldots, N-1 && \text{(collocation conditions)} \\
&x_c(k+1) - p_k(t_k, v_k)dh = 0, && k = 0, \ldots, N-1 && \text{(continuity conditions)} \\
&g(x_c, u_k) \leq 0, && k = 0, \ldots, N-1 && \text{(inequality constraints)} \\
&r(x_c(N)) \leq 0, && && \text{(terminal constraint)}
\end{aligned} \tag{3.73}$$

The problem is formulated using the CasaDi stack called opti in MATLAB. The solver then calls the Interior Point OPTimizer *IPOPT*, a software library often used for solving large NLPs.

4

Results

4.1 Model transient analysis

To analyze the behavior of the system, some transient responses were made for each of the six inputs. The system is *decoupled* unless stated otherwise to facilitate analysis. The general condition for each of the tests is a total horizon optimal control problem (with $T = 3600s$, $N = 120$, $h = 30s$), meaning an entire horizon is solved.

4.1.1 Heater/Chiller unit step responses

Starting off is a test where everything starts off with no external heating ($d_1 = d_2 = 0$), ambient temperature d_3 set to 40 $°C$, the volumetric flow rates u_3 and u_4 are set to their nominal lower bounds, the vehicle speed d_4 set to zero, and all other inputs (u_2, u_5, u_6) set to zero. This is followed by a step change of increased heat from the heater/chiller unit u_1 seen in Figures 4.1 and 4.2. Plots that would show the inputs and disturbances that are at rest are exempted to save page space. For all plots in the chapter holds $x = [T_B\ T_M\ T_1\ T_5]^T$.

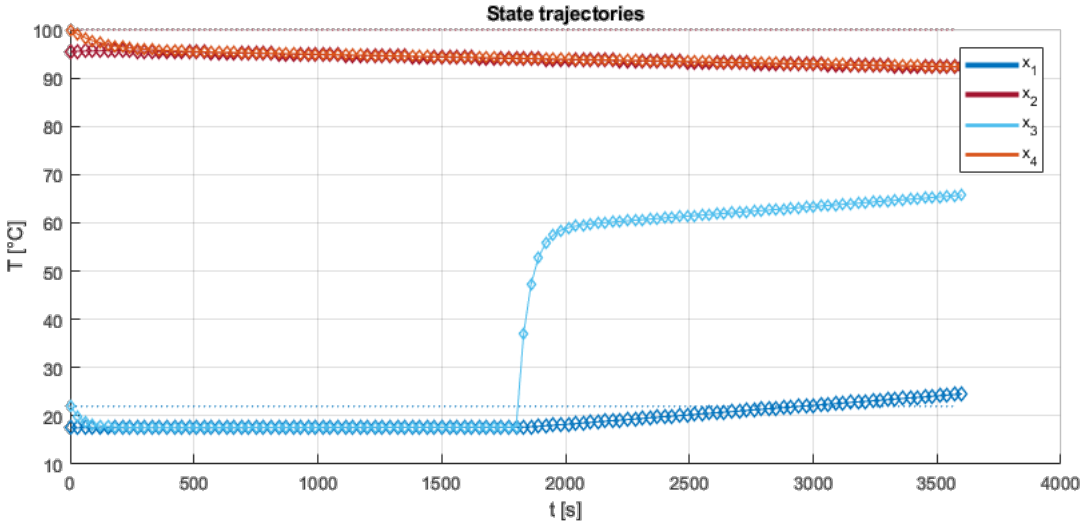

Figure 4.1: State trajectories when input u_1 is increased to 6000 joules per second at time 1800s.

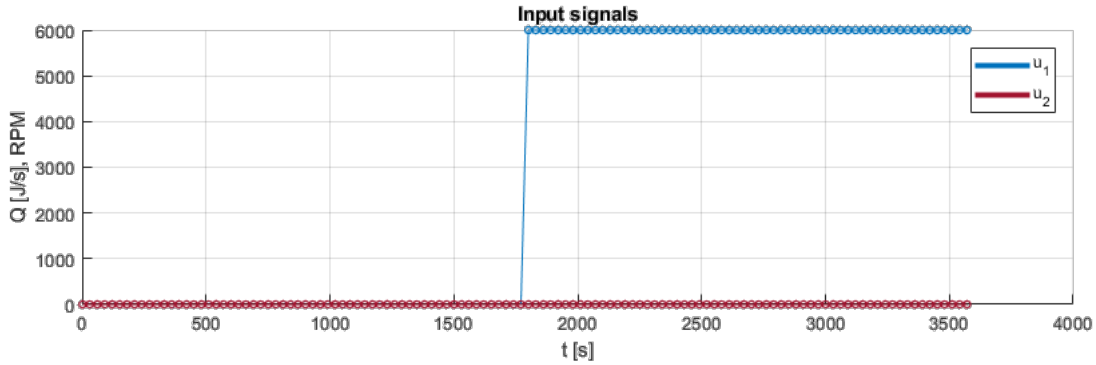

Figure 4.2: Step increase of input signal u_1 from 0 to 6000 joules per second at time 1800s.

The model response to the input change is an expected behavior. Increased heater/chiller unit heating should result in increased ESS coolant temperature x_3 and ultimately the ESS temperature x_1 itself. Before the step increase it can be seen that the temperatures slowly decrease due to heat dissipation to the environment. The test is repeated with the same starting conditions but with a negative u_1 step change instead, meaning the heater/chiller instead provides cooling. The negative effect value of course indicates heat is removed from the coolant.

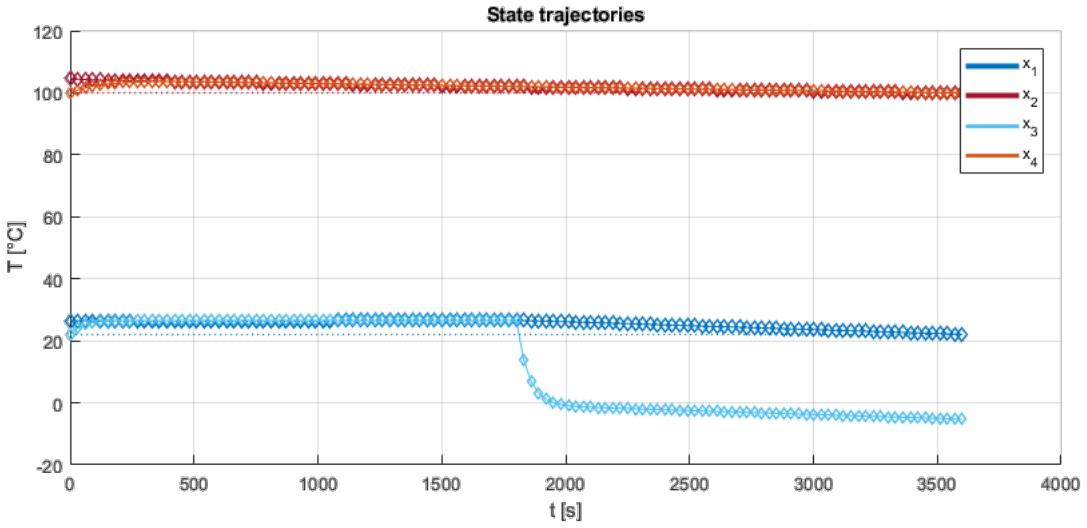

Figure 4.3: State trajectories when input u_1 is reduced to -6000 joules per second at time 1800s.

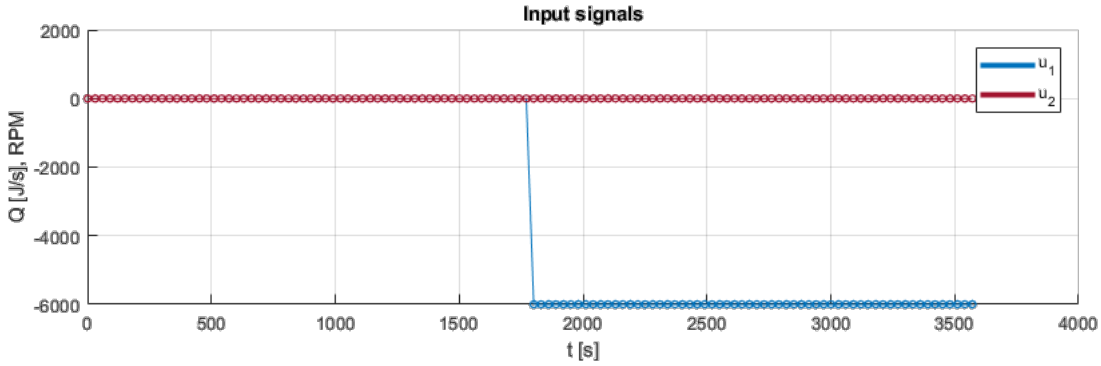

Figure 4.4: Step change of input signal u_1 from 0 to -6000 joules per second at time 1800s.

This test mirrors the previous with cooling instead of heating and is reflected in the state trajectories. The coolant temperature x_3 followed by ESS temperature x_1 are both reduced by the cooling. Both tests showcase that the coolant has less thermal inertia than the ESS.

4.1.2 Fan speed step response

The next input to be analyzed is the fan speed, known as input signal u_2. As for the tests with input u_1 before; the vehicle speed is set to zero, ambient temperature set to 40 $°C$, volumetric flow rates are set to their nominal lower bounds, external heating is set to zero and all inputs are set to zero except a step change on u_2.

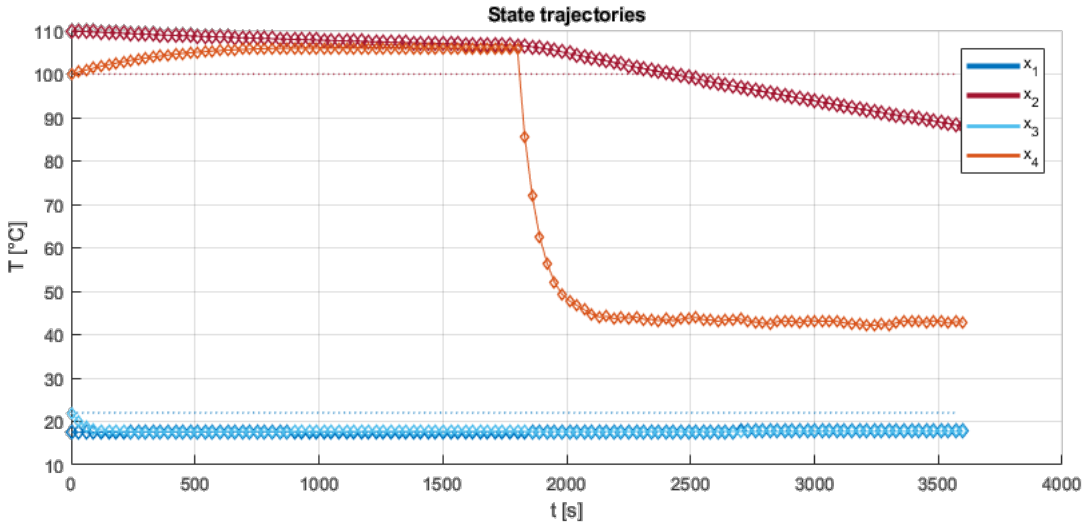

Figure 4.5: State trajectories when input u_2 is set to 600 RPM at time 1800s.

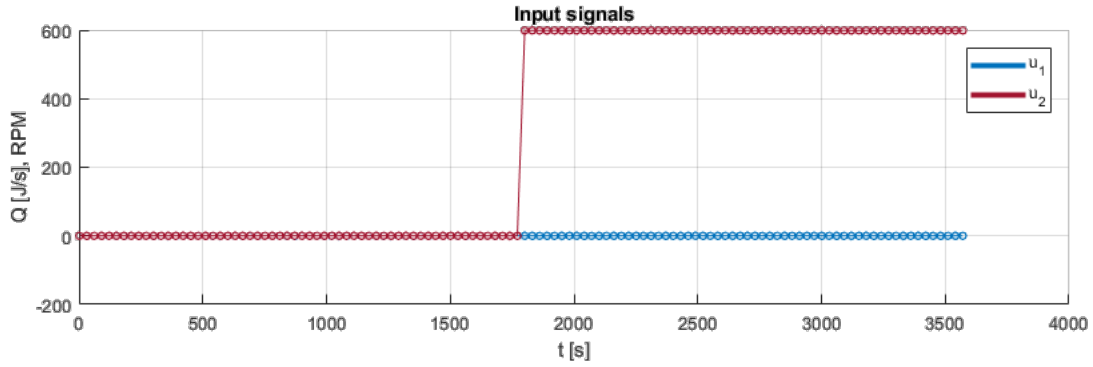

Figure 4.6: Step change of input signal u_2 from 0 to 600 RPM at time 1800s.

The input u_2 in decoupled mode does not impact the states x_1 and x_3 but instead the MDS temperature x_2 and MDS coolant temperature x_4. With current assumptions 600 RPM is the maximum fan speed, which forces x_3 to rapidly release heat through the radiator and approach the ambient temperature. The MDS temperature x_2 is simultaneously lowered.

4.1.3 Volumetric flow rates

4.1.3.1 ESS loop volumetric flow rate step responses

The next input to be considered is the volumetric flow rate of the ESS loop u_3. To better showcase its effect on the states, a constant heating value by u_1 is supplied. Everything else is at rest as stated in the tests before.

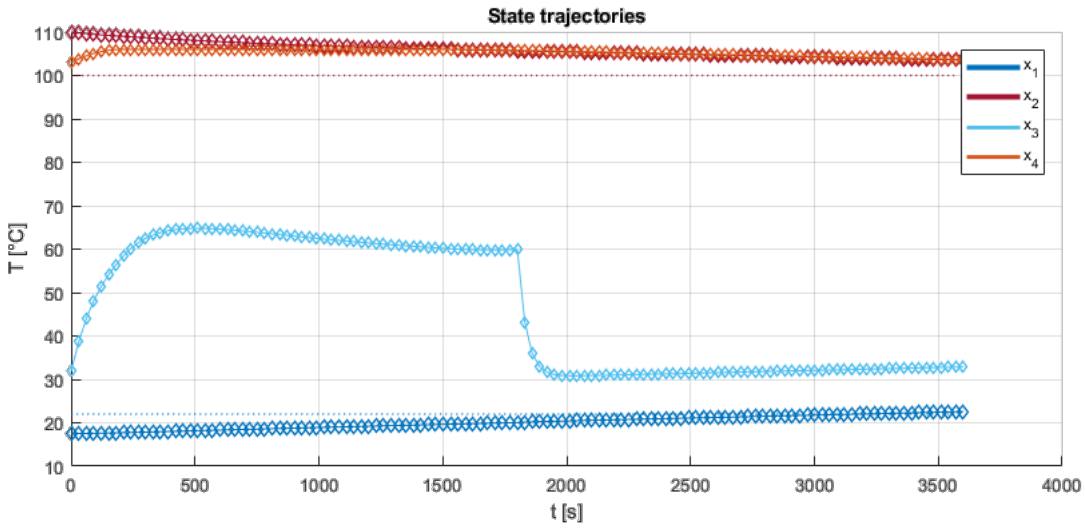

Figure 4.7: State trajectories when input u_3 is changed from 12 to 60 liters per minute at time 1800s.

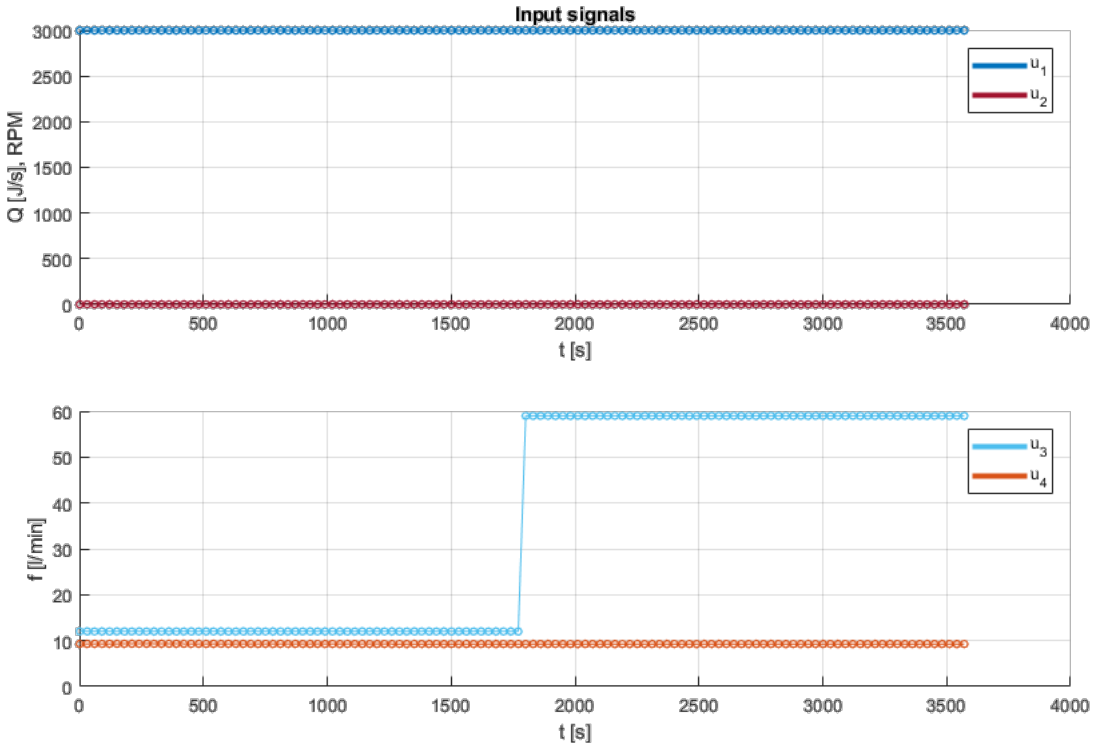

Figure 4.8: Input signal u_1 set to 3000 joules per second. Step change of input signal u_3 from 12 to 60 liters per minute at time 1800s.

Note that the initial value of u_3 in this test is lower than the nominal lower bound of 42 liters per second to provide clearer change in the plots for the reader. The system starts off being heated by u_1, which is seen by the increase of x_3. The sudden decrease of x_3 when u_3 is drastically increased is explained by the heat transfer coefficient h in the exchanger between the ESS and the coolant. The increased flow rate does not increase the thermal mass itself, but does increase the heat transfer coefficient h significantly as it is dependent on the flow speed. The coolant then absorbs the heat much faster from the ESS, making the two temperatures converge to a new thermal equilibrium. Without the heating supplied by u_1 this effect would be much less apparent because the coolant temperature would already have converged as is seen in the states x_2 and x_4 in Figure 4.7.

The test is repeated but with a decrease of u_3 instead, in essence a reverse case compared to before. The heating supplied by u_1 remains the same.

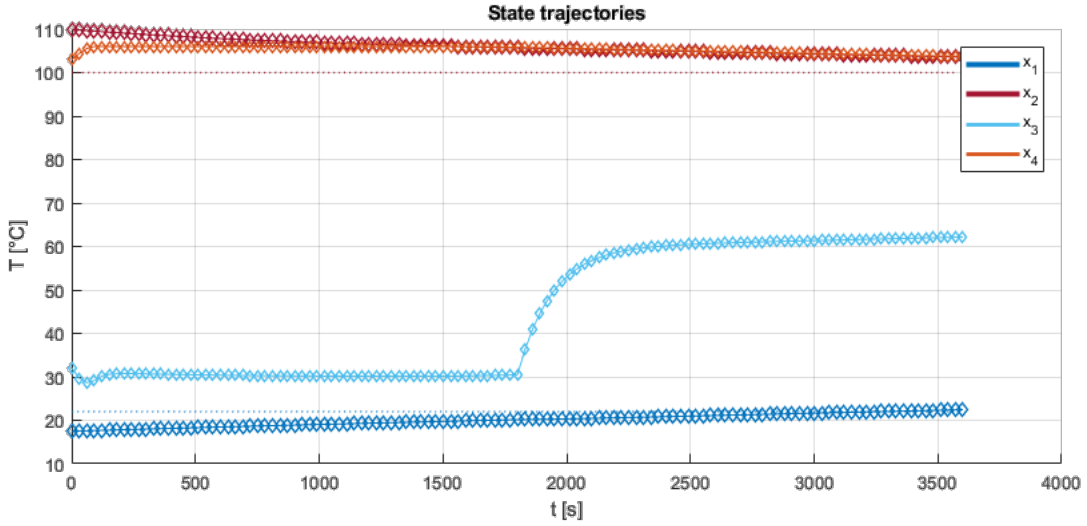

Figure 4.9: State trajectories when input u_3 is decreased to 12 from 60 liters per minute at time 1800s.

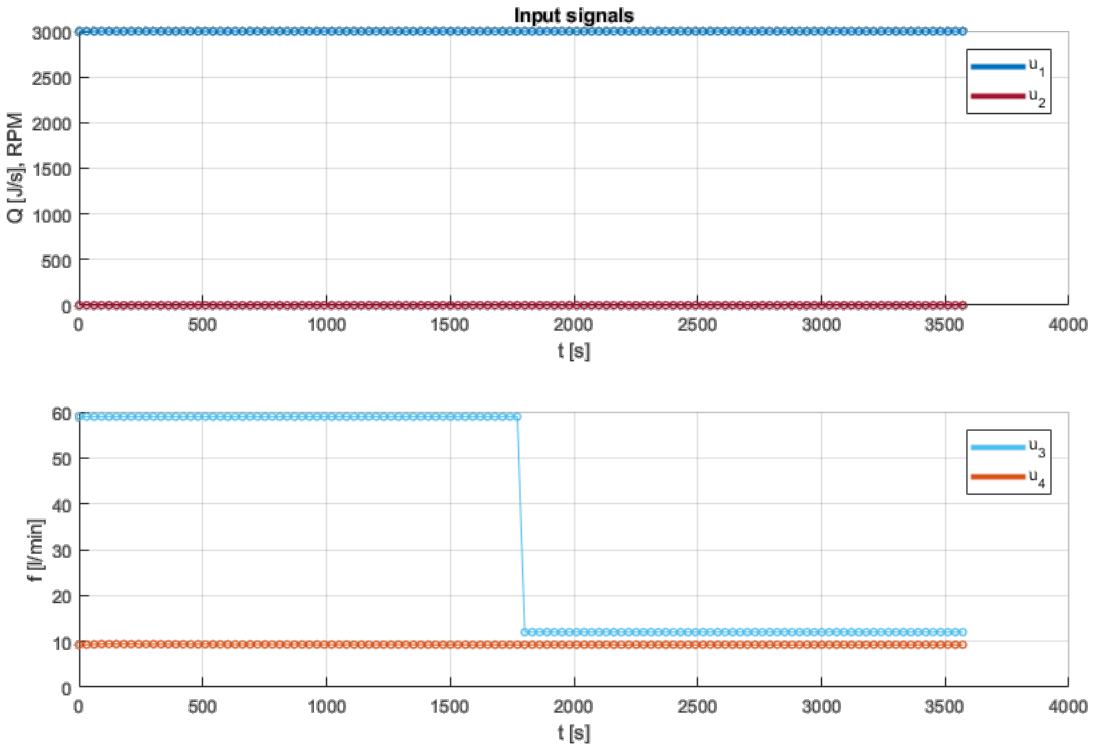

Figure 4.10: Input signal u_1 set to 3000 joules per second. Step change of input signal u_3 from 60 to 12 liters per minute at time 1800s.

The behavior is as expected, with the coolant temperature x_3 diverging from the ESS temperature x_1 as the flow rate u_3, and consequently h, decreases.

4.1.3.2 MDS loop volumetric flow rate step responses

Next is to analyze the volumetric flow rate in the MDS loop u_4. The tests will be done with a small amount of radiator cooling to better show the impact of the flow rate.

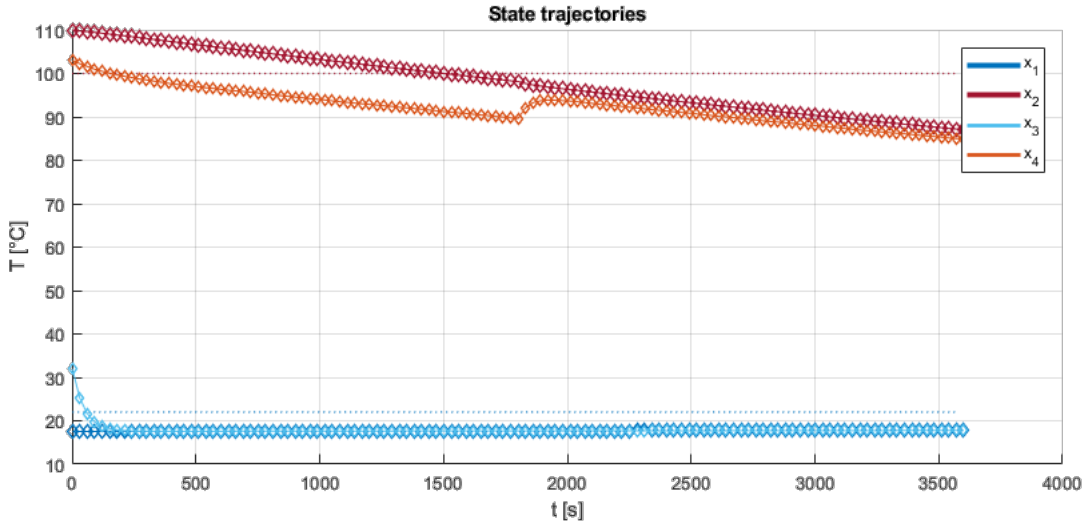

Figure 4.11: State trajectories when input u_4 is increased from 7 to 30 liters per minute at time 1800s .

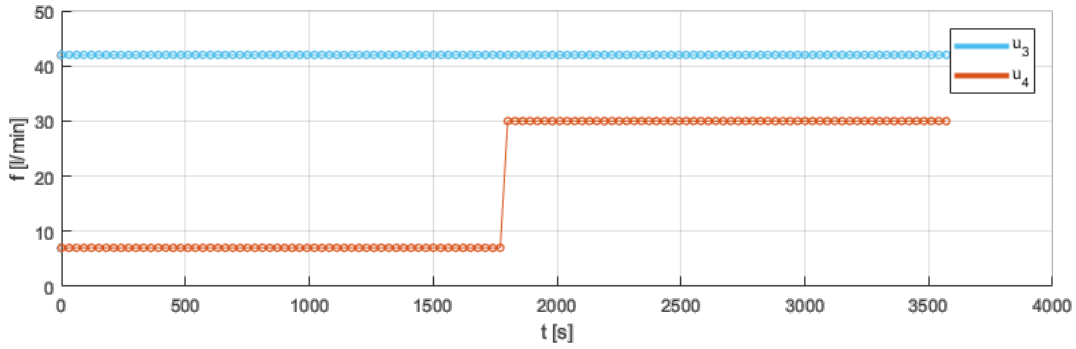

Figure 4.12: Step increase of input signal u_4 from 7 to 30 liters per minute at time 1800s.

The behavior is similar to the case for the ESS loop. Increased volumetric flow rate leads to higher heat transfer rate and convergence of the temperatures. The case of reducing the volumetric flow rate is shown.

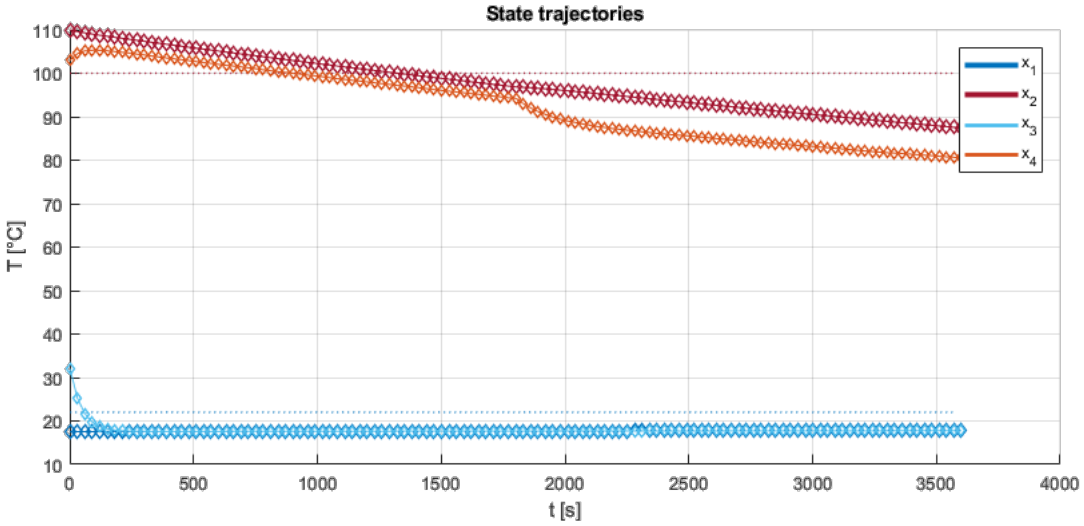

Figure 4.13: State trajectories when input u_4 is decreased from 30 to 7 liters per minute at time 1800s.

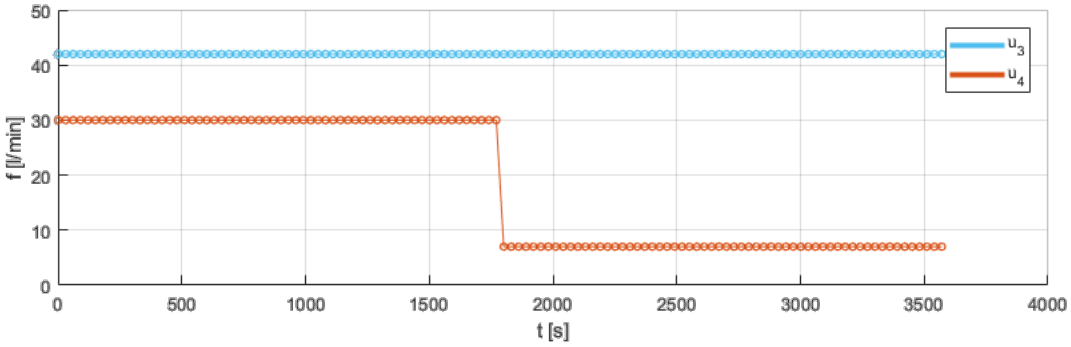

Figure 4.14: Step decrease of input signal u_4 from 30 to 7 liters per minute at time 1800s.

Yet again the behavior is shown. This time when the volumetric flow rate is decreased the temperatures diverge as the result of lower heat transfer rate.

4.1.4 Valves

For the decoupling valve variable u_5, more variables are free for the solver to set. A case where disturbances are included, as well as many inputs being free is showcased next. Note that vehicle speed is set to zero. The effect of the coupling of the two system loops is very apparent.

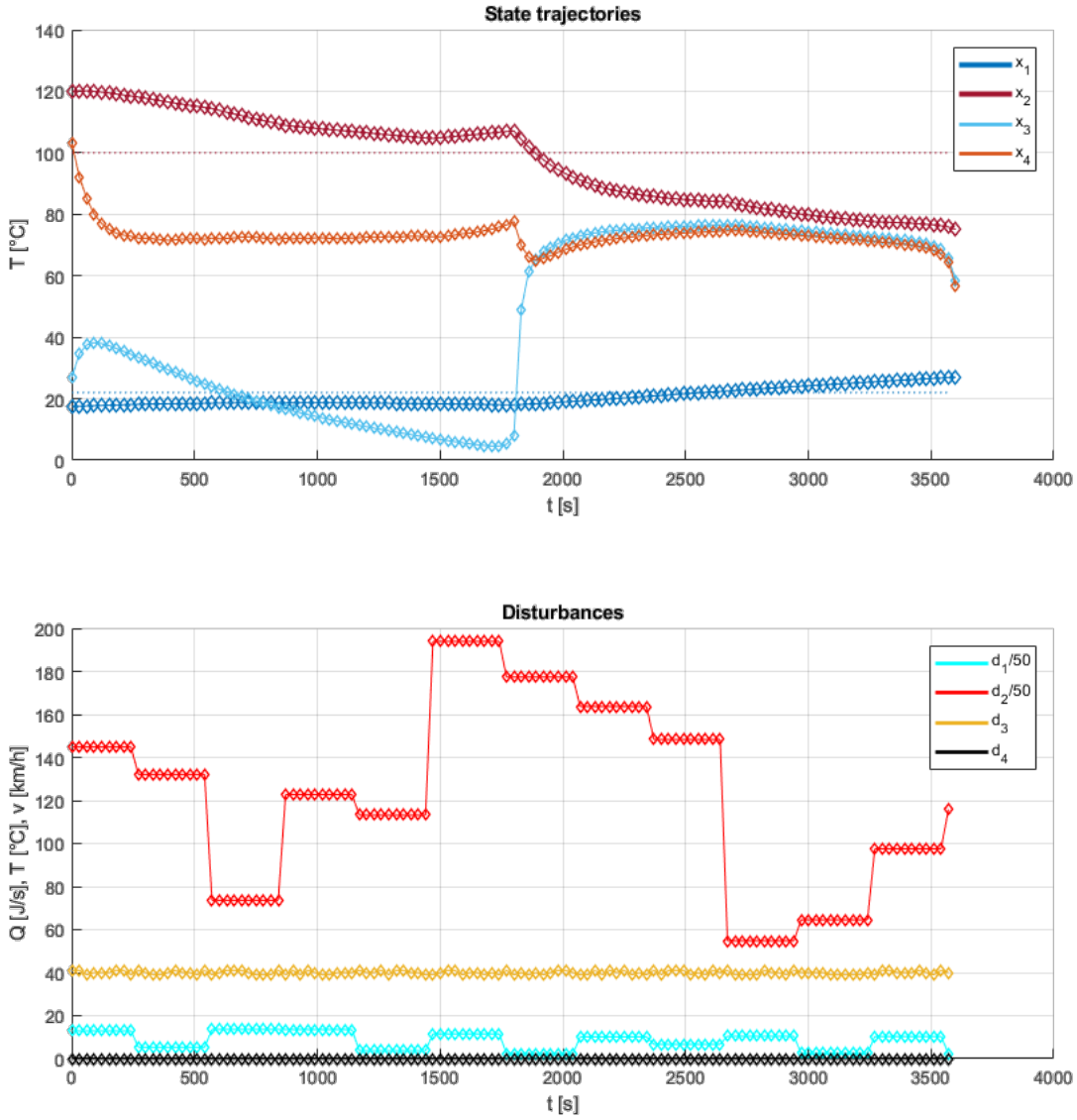

Figure 4.15: State trajectories when input u_5 at time 1800s is changed from 0 to 1 in the upper plot. System disturbances are shown in the lower plot with d_1 and d_2 being scaled down by a factor of 50 for a better fit in the figure.

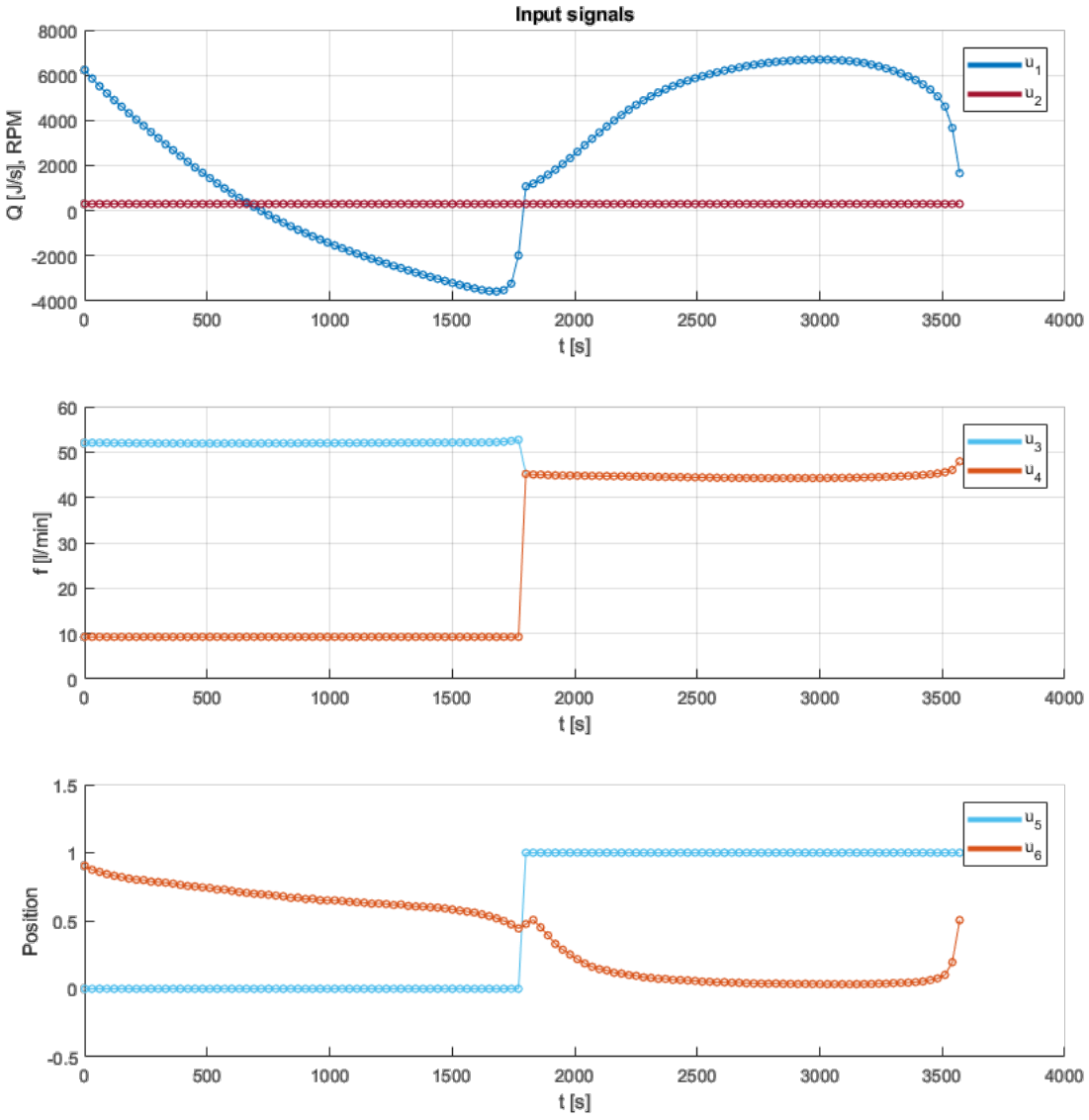

Figure 4.16: Step change of input signal u_5 at time 1800s from 0 to 1, along with the solver freely choosing the other input signals.

Even if there are many input changes at once, the effect of coupling the two loops is clearly visible in the behavior of the the coolant temperatures x_3 and x_4. After u_5 is set to 1 the two coolant temperatures rapidly converge towards each other. This behavior will be shown and discussed in greater detail in the receding horizon control section.

The last input signal to be analyzed is the radiator valve u_6. The benefit of the input signal is that the optimization solver may choose to reject radiator heat transfer. The next case involves a constant vehicle speed d_4 of 50 km/h to demonstrate the how the solver might regulate u_6 to better track the reference value of x_2.

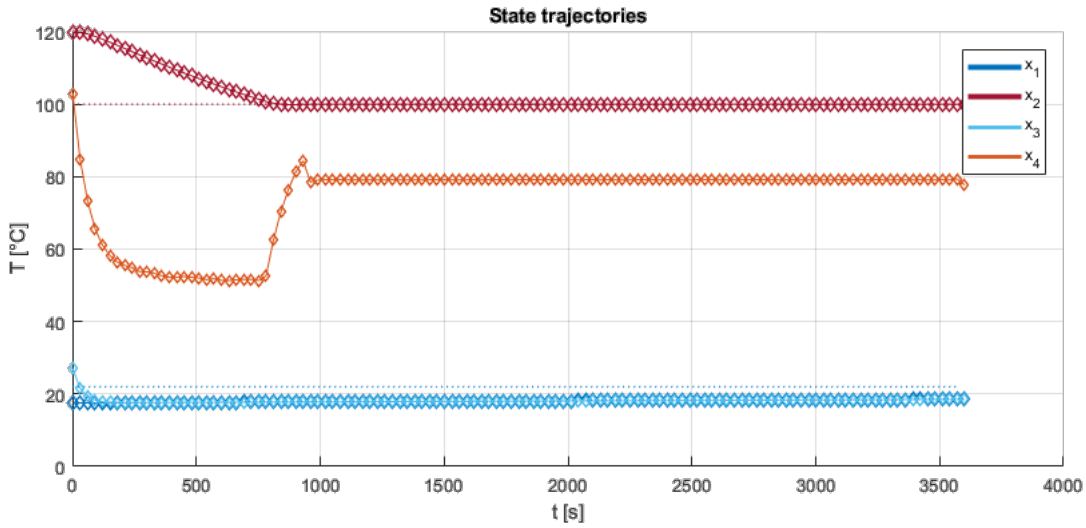

Figure 4.17: State trajectories when input u_6 is freely chosen by the solver.

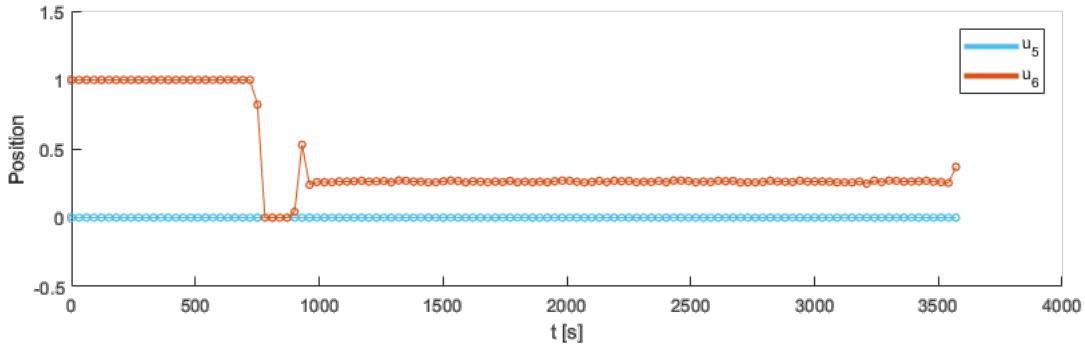

Figure 4.18: Input signals of the valves. The radiator valve u_6 values are chosen by the solver.

The solver clearly chooses to reject much of the ram-air heat dissipation through the radiator after the MDS temperature x_2 has reached the reference value of 100 $°C$. This shows that the cooling provided by the ram-air intake in fact can be dynamically utilized or rejected.

4.2 Receding horizon control

The next step is to implement the NLP solver in a RHC structure to continuously solve the optimization problem in a loop. The idea then is to utilize future disturbance information of the cooling system to predict optimal control ahead of time each time instance. The degree of the Legendre polynomials in the direct collocation was set to 2, as it struck an appropriate balance between solver accuracy and computation time.

Compared to a total horizon approach the system still calculates predicted states and optimal input signals but will now feed back the first optimal inputs and repeat the procedure. The OCP is free to utilize all inputs. Disturbances are generated as piecewise constant signals with a new random value every 300 seconds on the intervals

$$\begin{aligned} 100 \leq d_1 \leq 700, \quad & [Js^{-1}] \\ 2500 \leq d_2 \leq 12500, \quad & [Js^{-1}] \\ 39 \leq d_3 \leq 41, \quad & [^\circ C] \\ 5 \leq d_4 \leq 90, \quad & [kmh^{-1}]. \end{aligned}$$

The reference values for the ESS and MDS are in degrees Celsius defined as

$$r = [22 \quad 100]. \tag{4.1}$$

The initial conditions for the states are

$$x_0 = [r_1 \quad r_2 \quad r_1 + 5 \quad r_2 + 5], \tag{4.2}$$

meaning that the ESS and MDS both start at their reference values, and the coolants five degrees Celsius higher. The objective function was continuously tuned until arriving at

$$\begin{aligned} \min \quad & J(x,u) = \\ & \sum_{0}^{N-1} \Big(10^{-4} u_1(k)^2 + 10^{-3} u_2(k)^2 + 10^6 u_3(k)^2 + 10^6 u_4(k)^2 + 10^2 (x_1(k) - r_1)^2 + 20 (x_2(k) - r_2)^2 \Big) \\ & \quad + 5 \cdot 10^6 (x_1(N) - r_1)^2 + 2.5 \cdot 10^5 (x_2(N) - r_2)^2. \end{aligned} \tag{4.3}$$

This tuning heavily prioritizes reference tracking of the ESS. The weights of the inputs are scaled to become of similar magnitude to aid the solver. There are notably large weights on the terminal weights than the stage cost weights. This allows the solver to temporarily deviate from the reference value in certain cases which is useful for anticipating high heat generation by pre-cooling ahead of time.

Four cases with a constant step size $h = 30s$ will be demonstrated. The final time t_f for each case is 1800 seconds (15 minutes), which gives a total number of $1800/30 = 60$ iterations in each run. The horizon length T and number of control points N are increased for each case. The first case considered is with a horizon $T = 120s$ and control points $N = 4$. Solid lines in the plots indicate past values, and the diamond points indicate predicted values.

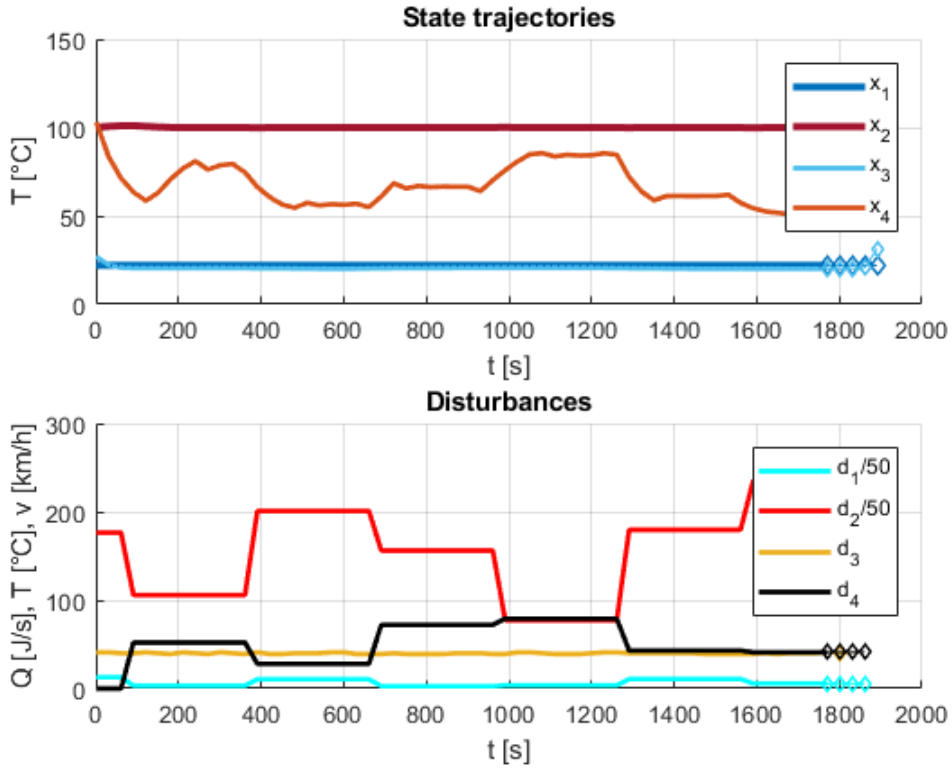

Figure 4.19: RHC state trajectories and disturbance values; $T = 120s$, $N = 4$, $h = 30s$.

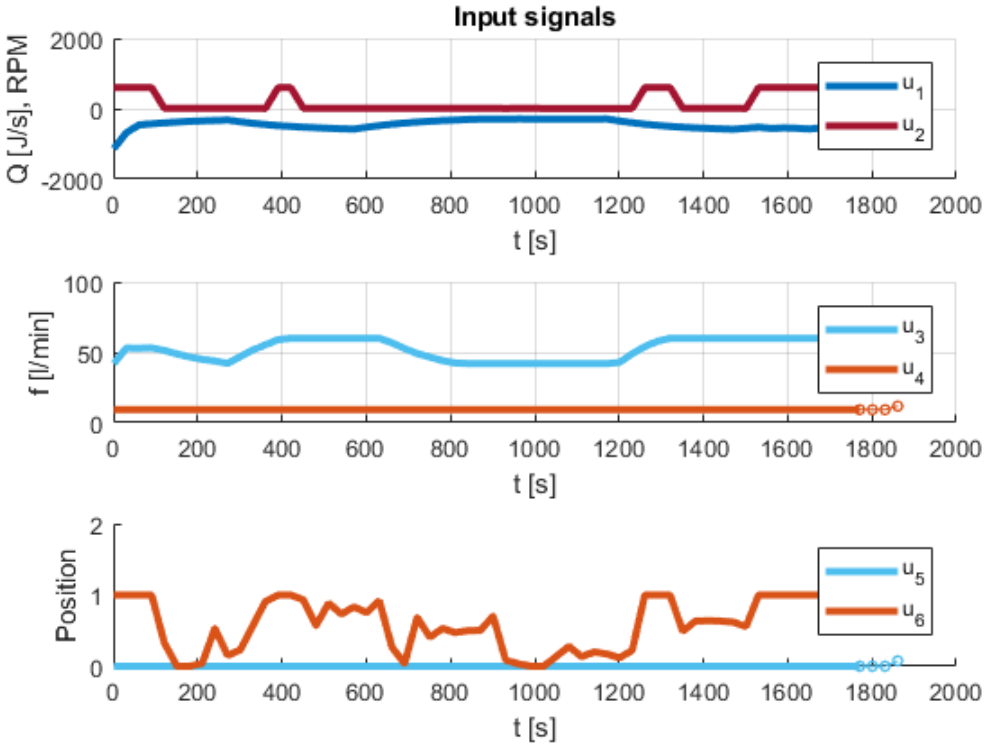

Figure 4.20: Input signal vectors for the RHC run with $T = 120s$, $N = 4$, $h = 30s$.

The system is able to track the reference values with good accuracy despite the changing conditions in the disturbances. The prediction horizon is however shorter (120s) than the disturbance generation time (300s), meaning the RHC cannot predict farther than one step change at any given time. The system usually does not utilize coupling when close to a steady-state condition. The ESS temperature x_1 is heavily regulated by means of u_1 and u_3 in the decoupled state. The MDS temperature x_2 is sufficiently controlled by a combination of utilizing the fan speed u_2 and ram-air cooling control by the radiator valve u_6. A plot providing the computation time of each iteration is provided in Figure 4.21.

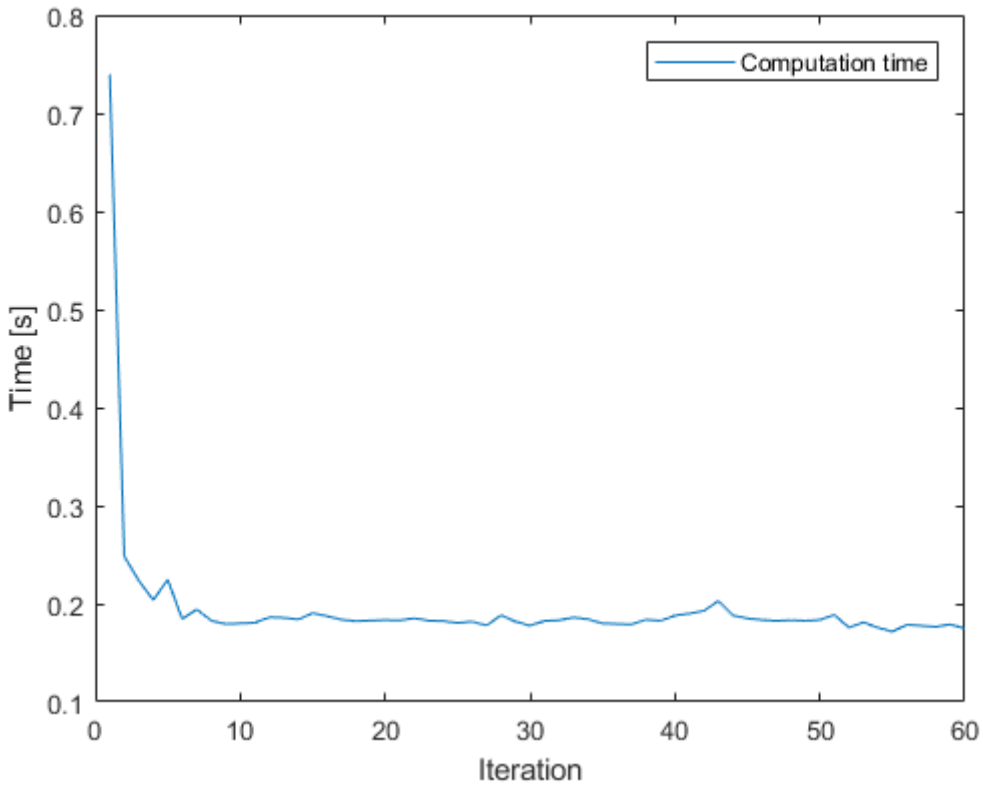

Figure 4.21: Computation time for each iteration in the RHC run with $T = 120s, N = 4, h = 30s$.

The overall computation time for this case of relatively low resolution is low. Computation time drops to around 0.2 seconds after the first few iterations. This is due to the optimization solver making better initial guesses with further iterations. The cumulative sum of cost function J for the 60 iterations was determined as:

$$J_{tot} = \sum_{t=0}^{t_f} J(x, u) = 2.79 \cdot 10^5. \tag{4.4}$$

The context of the value of J_{tot} will be made more clear after the four cases have been presented. In the next case the horizon and number of control points are increased to $T = 300s$ and $N = 10$.

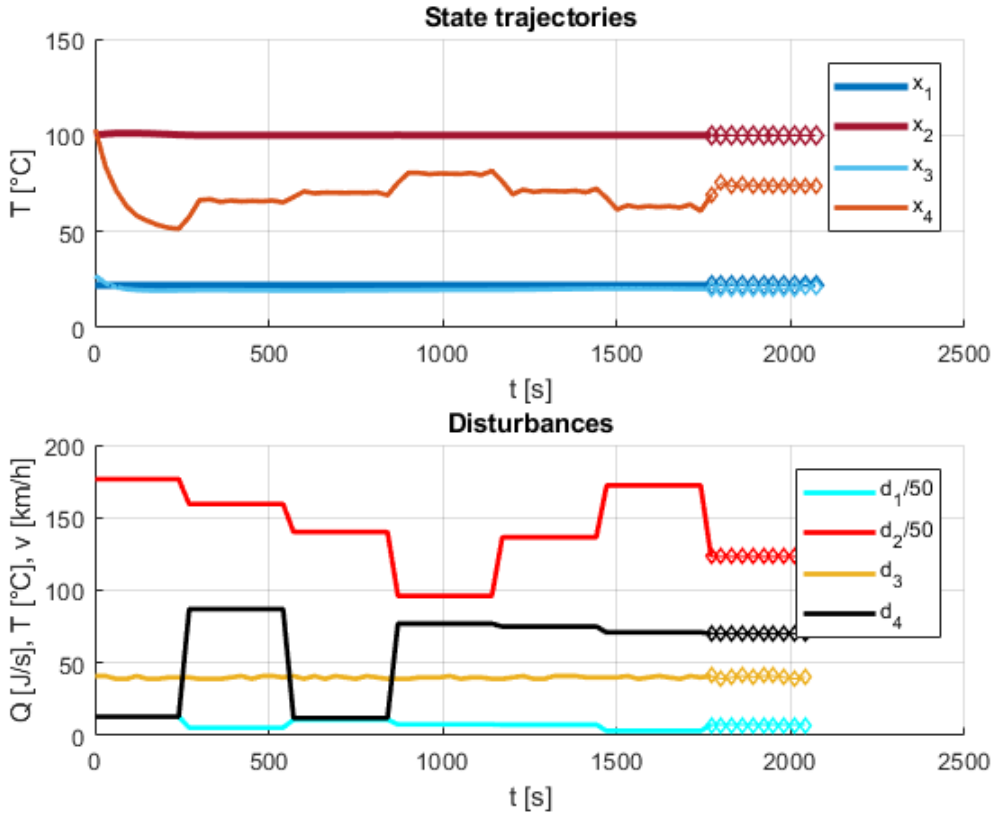

Figure 4.22: RHC state trajectories and disturbance values; $T = 300s$, $N = 10$, $h = 30s$.

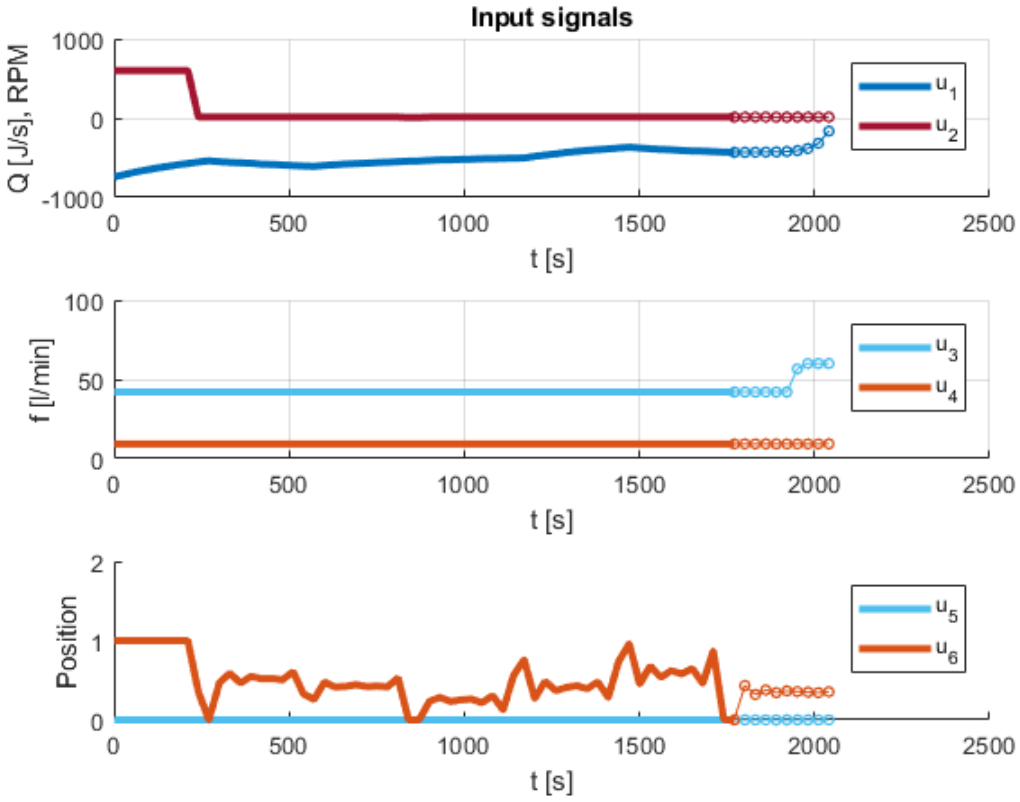

Figure 4.23: Input signal vectors for the RHC run with $T = 300s$, $N = 10$, $h = 30s$.

The overall behavior is similar to the previous case. However the increased horizon length now matches the disturbance generation sampling rate, which is reflected in the trajectory of x_4. The coolant temperature is smoother and corresponds better to the changes in d_2. The computation time for this case is shown in Figure 4.24.

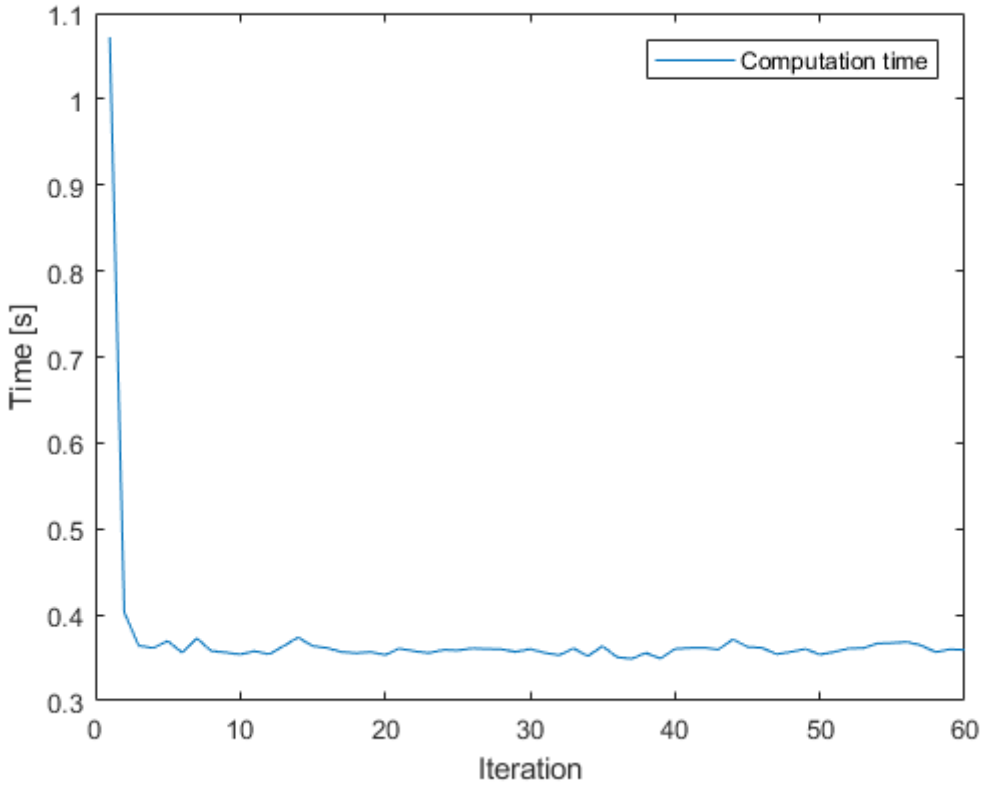

Figure 4.24: Computation time for each iteration in the RHC run with $T = 300s, N = 10, h = 30s$.

Computation time can still be considered very low, but is almost twice as high overall compared to the previous case by converging to slightly lower than 0.4 seconds. This can indicate that resolution and horizon length may be increased even more while still being lower than the step size. The cumulative cost function J_{tot} had the value of:

$$J_{tot} = \sum_{t=0}^{t_f} J(x, u) = 6.19 \cdot 10^5. \tag{4.5}$$

At first glance this seems worse than before, but the increased horizon naturally also increase the cost function value. The next case increases the horizon to $T = 1200s$ and control points to $N = 40$.

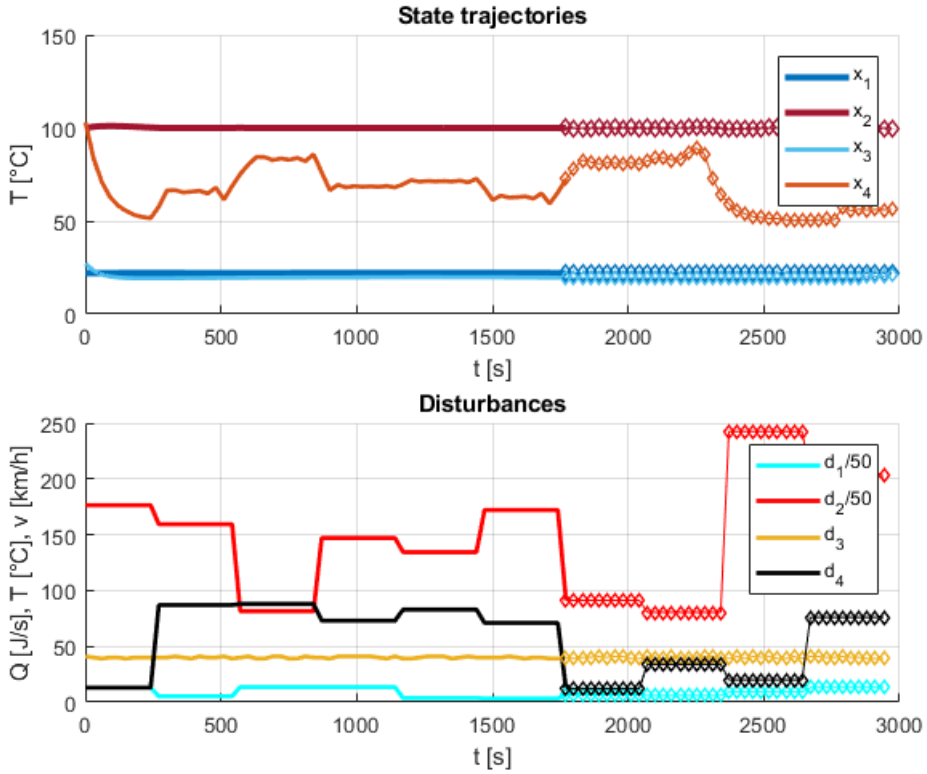

Figure 4.25: RHC state trajectories and disturbance values; $T = 1200s$, $N = 40$, $h = 30s$.

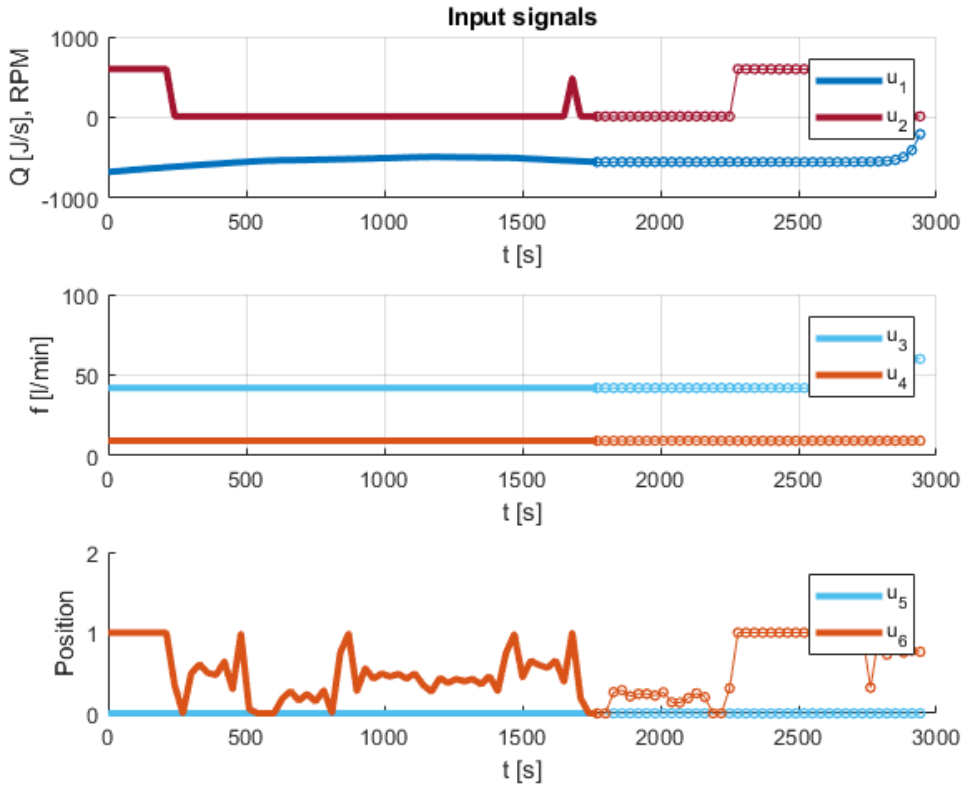

Figure 4.26: Input signal vectors for the RHC run with $T = 1200s$, $N = 40$, $h = 30s$.

With a prediction horizon of 20 minutes the RHC can utilize a lot of future disturbance information. The MDS coolant temperature x_4 is even smoother than before. It can be seen that a very large amount of heat generated by the MDS is predicted at time $t = 2300$. The fan speed u_2 is increased ahead of time to pre-cool the temperature of x_4 to mitigate reference deviation of x_2. This is precisely the behavior that demonstrates the potential of a receding horizon controller. The computation time for each iteration is once again provided:

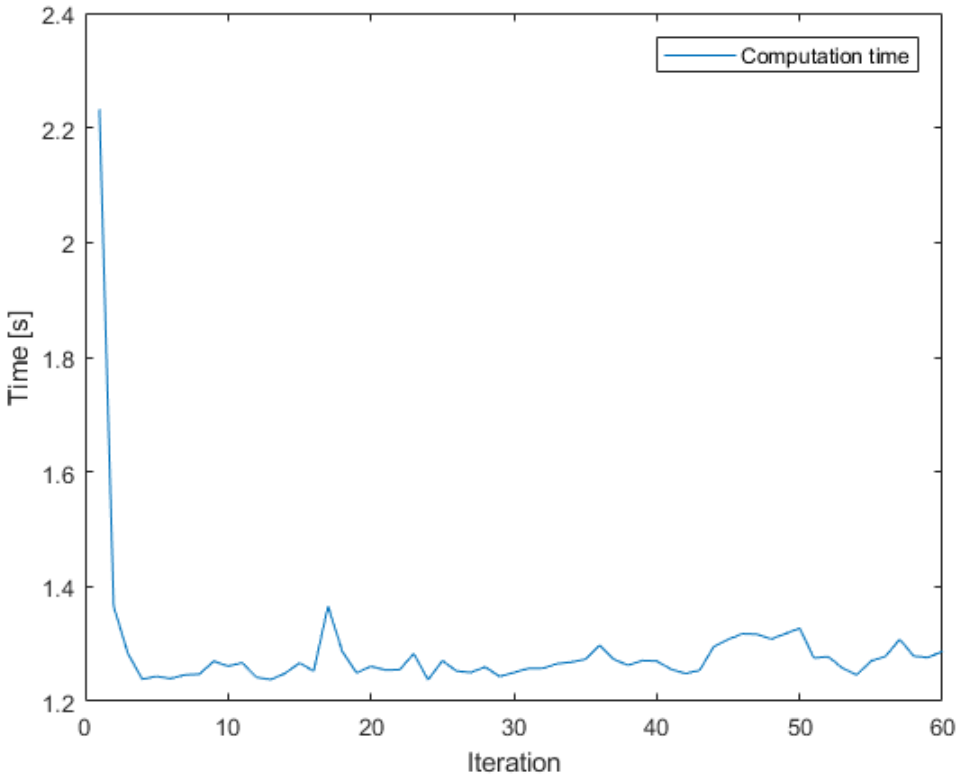

Figure 4.27: Computation time for each iteration in the RHC run with $T = 1200s, N = 40, h = 30s$.

Computation time is now consistently above one second per iteration at approximately 1.3 seconds. The cumulative cost function J_{tot} was calculated as:

$$J_{tot} = \sum_{t=0}^{t_f} J(x, u) = 2.25 \cdot 10^6. \tag{4.6}$$

The next and final case of this near-steady-state analysis increases the horizon to $T = 3600s$ and control points to $N = 120$.

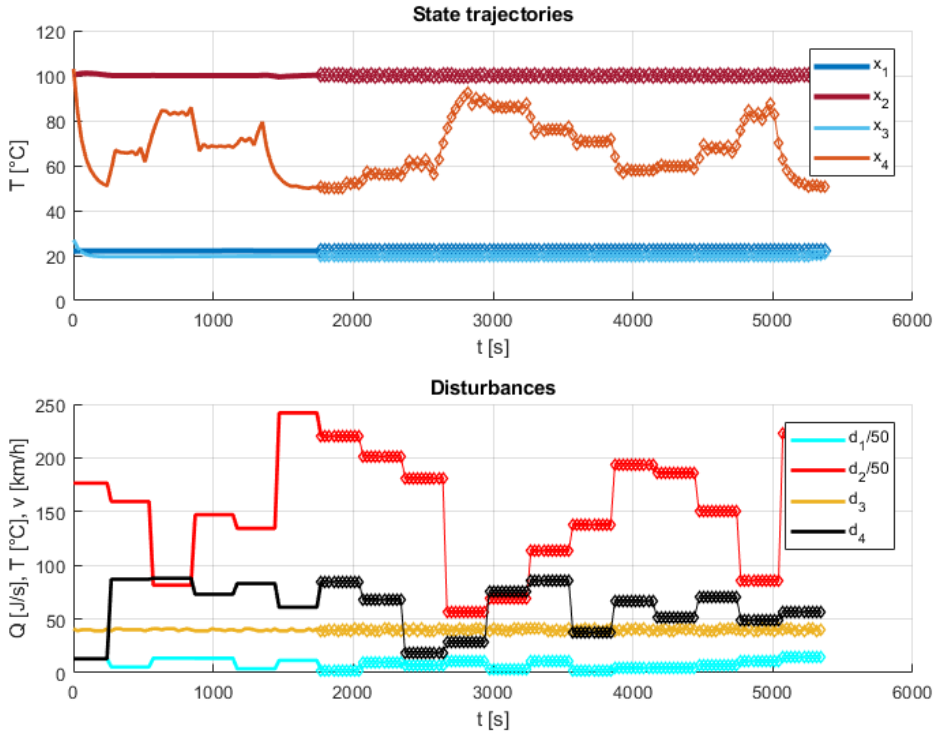

Figure 4.28: RHC state trajectories and disturbance values; $T = 3600s$, $N = 120$, $h = 30s$.

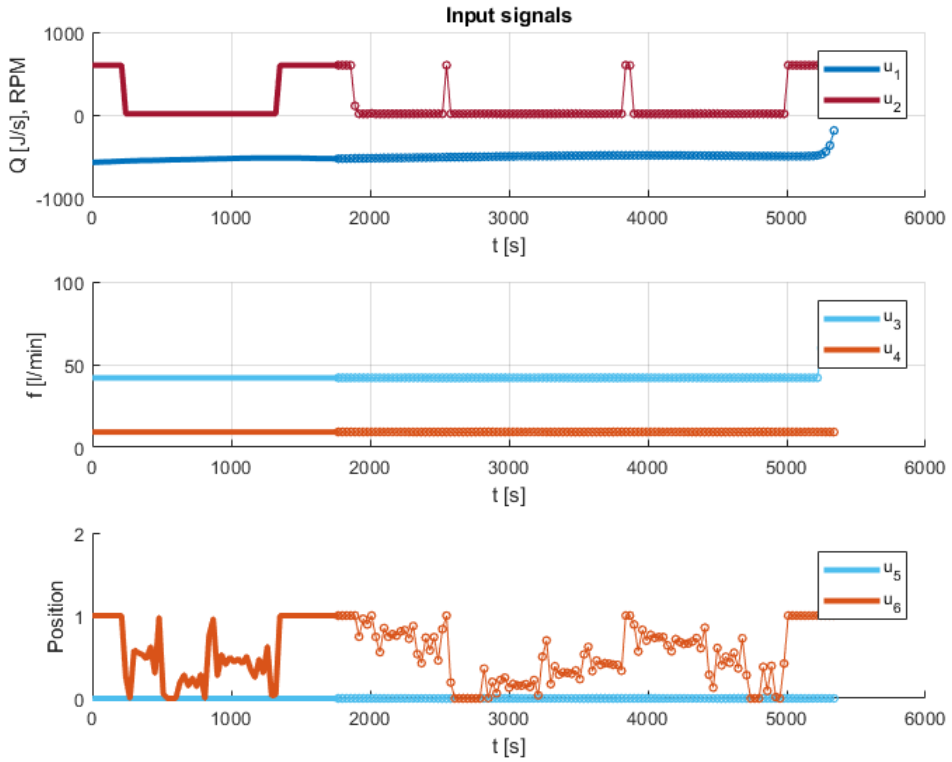

Figure 4.29: Input signal vectors for the RHC run with $T = 3600s$, $N = 40$, $h = 30s$.

The advantage of a prediction horizon is very clear in this case with an hour long horizon. The system anticipates many future changes in the disturbances, tracking the references while minimizing the input signals. The behavior is still most apparent in the MDS coolant temperature x_3. The computation time for this case is much higher than the previous cases, and also more erratic as can be seen in Figure 4.30.

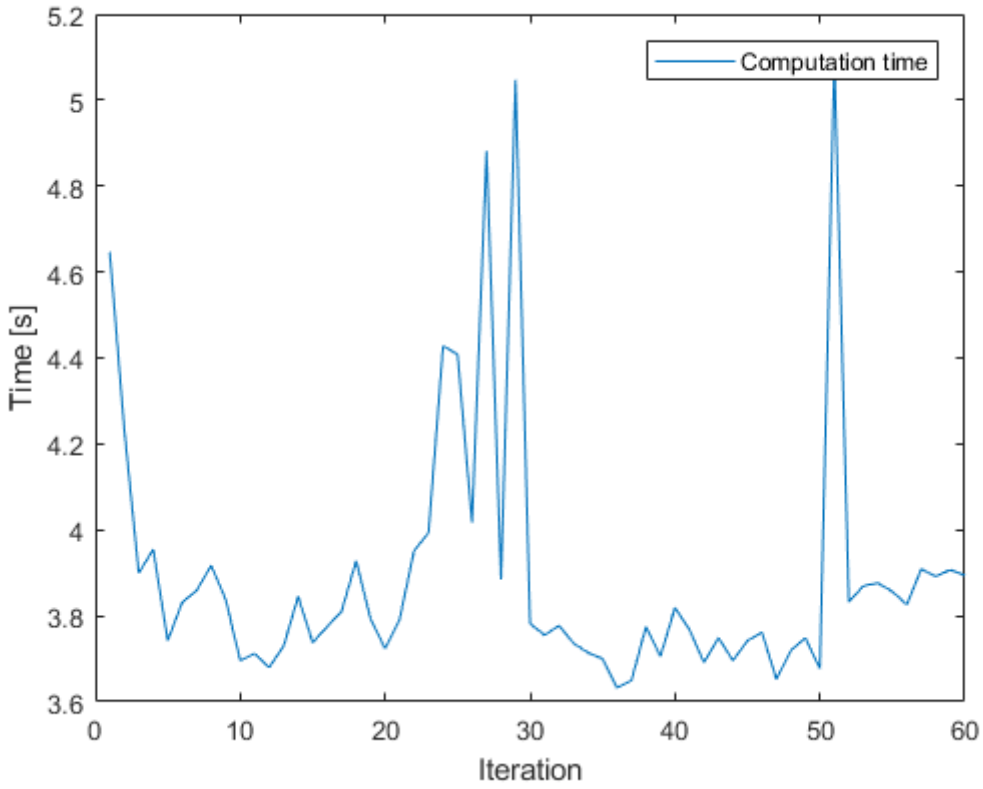

Figure 4.30: Computation time for each iteration in the RHC run with $T = 3600s, N = 120, h = 30s$.

The ability for an embedded processor to compute control signals in real-time may not be feasible for the scale of this case. Lastly, the cumulative cost function J_{tot} was calculated as:

$$J_{tot} = \sum_{t=0}^{t_f} J(x, u) = 5.58 \cdot 10^6. \tag{4.7}$$

The next subsection gives better perspective of the cumulative cost functions calculated for the different horizon lengths $T = 120s$, $300s$, $1200s$, $3600s$.

4.2.1 Objective function comparisons

The objective functions calculated in the previous section are hard to compare to eachother directly because J naturally increases as the horizon length T does. To better compare the cumulative objective function values from the four cases a normalized value for each objective function is calculated. The calculation is inspired from an average cost function expression from Mattingley et al. [27].

$$J_{avg} = \frac{1}{T} J_{tot} \tag{4.8}$$

$$\begin{aligned} J_{avg}^{T=120s} &= 2.33 \cdot 10^3 \\ J_{avg}^{T=300s} &= 2.06 \cdot 10^3 \\ J_{avg}^{T=1200s} &= 1.88 \cdot 10^3 \\ J_{avg}^{T=3600s} &= 1.55 \cdot 10^3. \end{aligned} \tag{4.9}$$

It can clearly be seen that the average value of the cost function decreases as the horizon increases. This implies that the ability of the receding horizon controller to minimize the cost function becomes better as the horizon increases. Of course, the computational resources required also increase with increased horizon length. Yet, it is clearly beneficial to anticipate future values of the system.

4.2.2 Decoupled versus coupled mode

There is a particular case that clearly showcases the advantage of allowing coupling between the two loops. The initial conditions are defined as follows:

$$x_0 = [r_1 - 4.5 \quad r_2 + 20 \quad r_1 + 5 \quad r_1 + 5] \tag{4.10}$$

The initial conditions then pose a problem; the ESS temperature x_1 is too low and the MDS temperature x_2 is too high. The decoupled case is demonstrated first (see Figures 4.31 and 4.32).

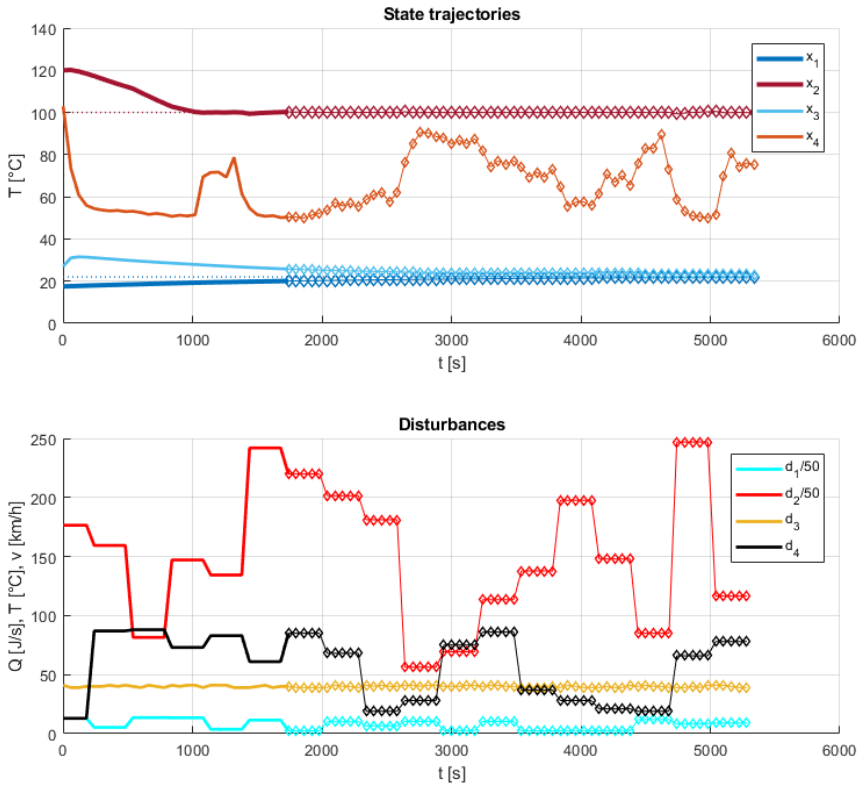

Figure 4.31: State trajectories and disturbance values for the decoupled case. $T = 3600s$, $N = 60$, $h = 30s$.

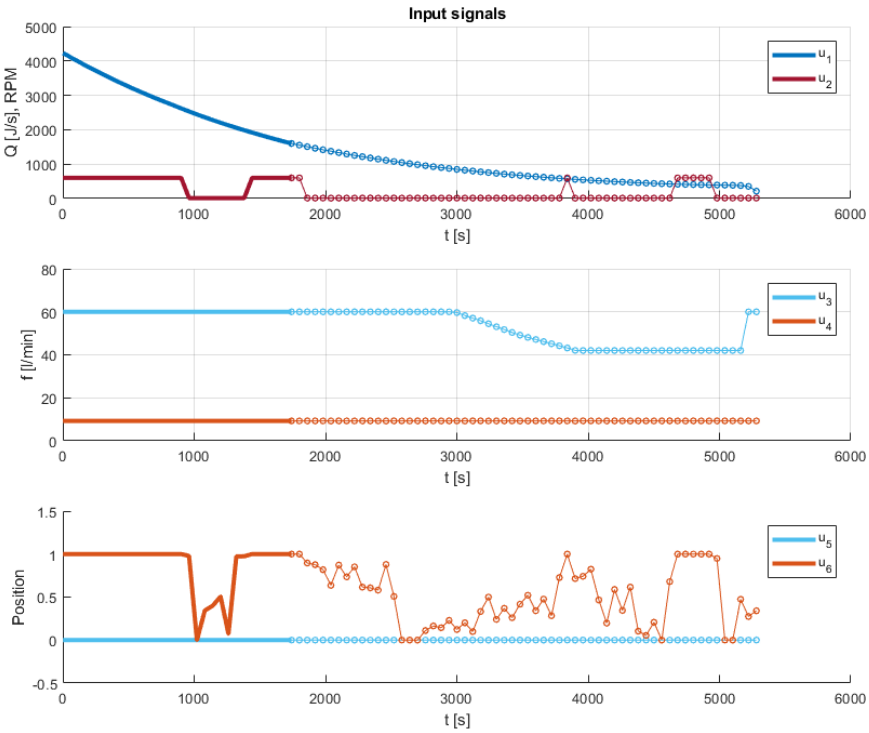

Figure 4.32: Input signals for the decoupled case. $T = 3600s$, $N = 60$, $h = 30s$.

The initial reference deviations are corrected by employing high heating from u_1 to heat the ESS. The MDS is cooled by saturating the fan speed u_2 and radiator valve u_6. The cumulative cost function value is calculated to be:

$$J_{tot} = 7.20 \cdot 10^7. \tag{4.11}$$

For the coupled case the solver may decide to set the coupling variable u_5 to a value between $0 < u_5 < 1$, which would cause the two coolant temperatures to quickly converge together. For this case where one component starts off too warm and the other too cold, the solver recognizes the benefit of coupling which allows for faster convergence to the reference values (see Figure 4.33).

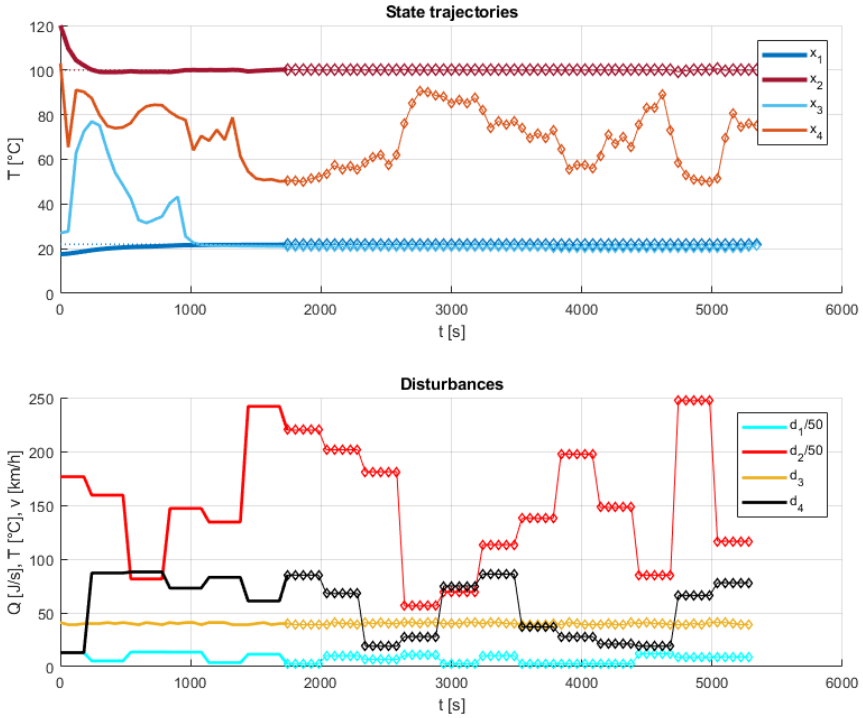

Figure 4.33: State trajectories and disturbance values for the coupled case. $T = 3600s$, $N = 60$, $h = 30s$.

The solver does indeed choose to couple the system initially. It can be seen that the control signal u_1 in Figure 4.34 is much lower than the coupled case, yet the reference for the ESS temperature x_1 is reached faster than before. Likewise the control signal for the fan speed u_2 is much lower overall and the MDS temperature reference is reached faster than before! There is also a clear difference in the cumulative cost function value:

$$J_{tot} = 3.16 \cdot 10^6. \tag{4.12}$$

This value is approximately only 4% of the J_{tot} of the decoupled run, which indicates much better cost function minimization overall when coupling is allowed. The solver

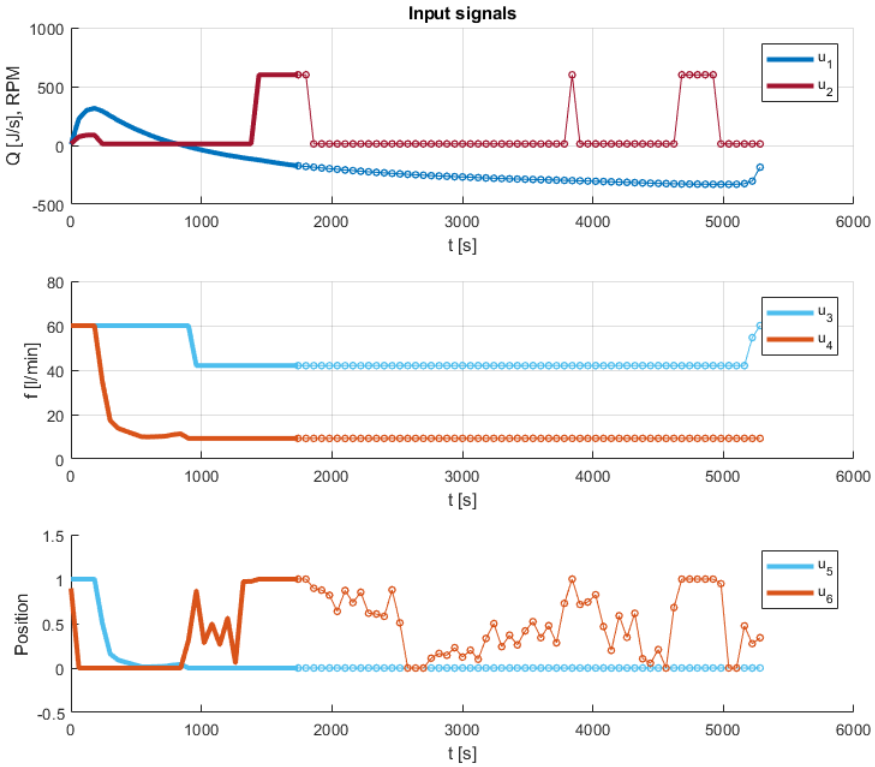

Figure 4.34: Input signals for the coupled case. $T = 3600s$, $N = 60$, $h = 30s$.

does not usually couple the thermal system when the state trajectories are predicted to track the references in a proper way. Real-world scenarios where unexpected temperature changes could happen may increase the occurrence of coupling.

4.2.3 Preliminary cooling

One of the prospects of a receding horizon controller with a sufficiently long prediction horizon is preparing the thermal system ahead of time for large heat generation spikes. Below is an example where very high heat generation is forced between times $3900s \leq t \leq 4500s$ (see Figure 4.35).

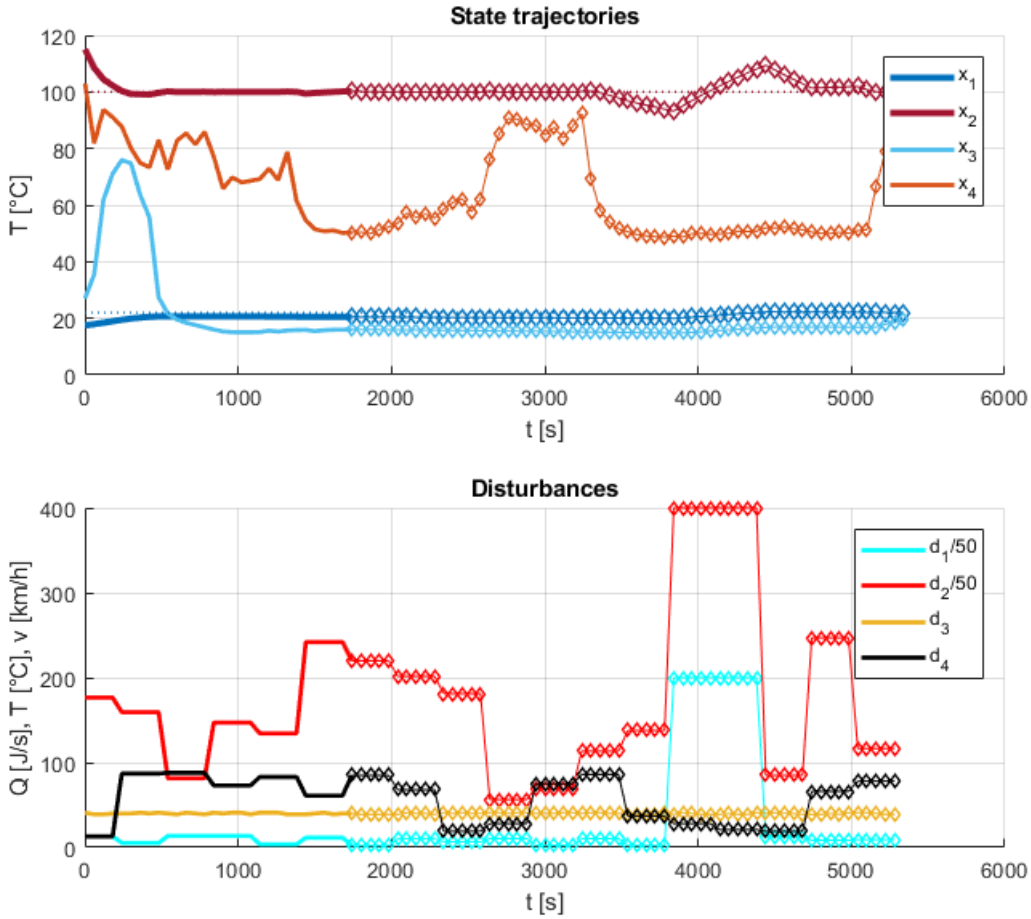

Figure 4.35: State trajectories and disturbance values for the coupled case that demonstrates preliminary cooling. $T = 3600s$, $N = 60$, $h = 30s$.

The expected behavior can clearly be seen by the predicted states of x_2. Even before the heat spike is expected to hit, the solver reduces the temperature of x_4 and subsequently x_2. The MDS temperature starts deviating significantly from the reference value, followed by utilizing the external heat to achieve a value that is almost averaged out around the reference. The solver calculates a similar trajectory for the ESS temperature x_1 but is not as apparent because of the prioritization to

keep excellent reference tracking. Also, the control signal u_1 starts to cool early, ahead of the disturbance.

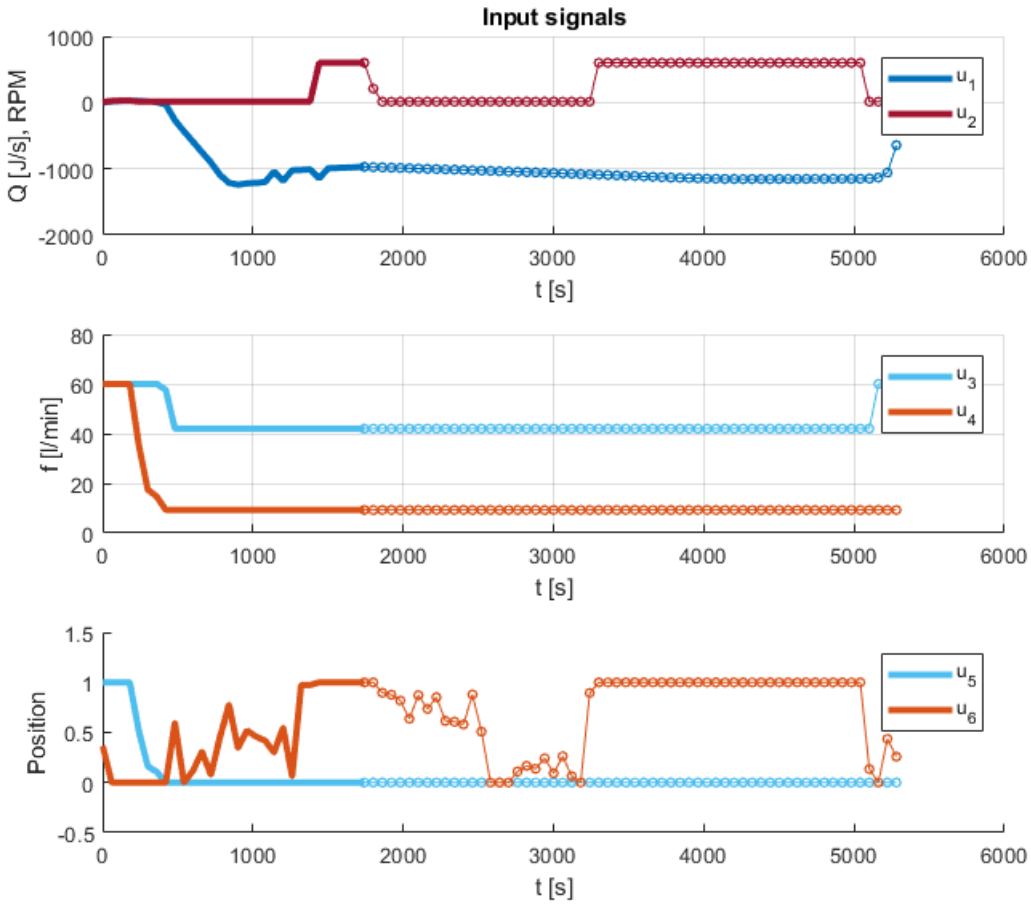

Figure 4.36: Input signals for the coupled case that demonstrates preliminary cooling. $T = 3600s$, $N = 60$, $h = 30s$.

5
Discussion

The results show compelling benefits of the receding horizon controller concept. Anticipating future disturbances shows great promise of reducing the value of the cost function. Having a centralized controller for the entire system also gives the opportunity to test the impact of various variables at once. The first research question can then be answered quite clearly: It is possible to successfully simulate and control the entire system in a receding horizon control strategy. The third research question is implicitly answered from the system model. Modelling the valves as continuous signals was possible and works with the solver, though the output is sensitive to the valve positions.

The final controller structure presented may be tuned in various ways to adjust the performance in different desired directions. It may be tuned to favor low total energy usage which would improve the range of the BEV. The OCP could on the other hand favor reference tracking instead, opting for the longevity of the components. The theoretical trade-off that was made in Equation 4.3 does place higher weights on the reference tracking, especially for the ESS.

5.1 The physical model

As with any mathematical representation of reality, there is model error to be determined by comparing with real-world scenarios. There are several potential areas of improvement for both the physical modelling and the control strategy itself. The main components of the modelling were the ESS, MDS and radiator. Each of these were modelled as relatively elementary heat exchangers under numerous assumptions, such as assuming certain geometry and physical parameters. The possibilities of future improvement of the accuracy of the models are great. For example, investigating the individual components could allow for utilization of advanced heat exchanger theory. The other direction is also possible; finding additional reasonable simplifications to render the complete model less complex. The derivations for the coolant temperatures were also made by assuming several ideal conditions, such as perfect mixing in the control volume and temperature invariant fluid parameters.

The current assumptions about the air speed surrounding the radiator are subjected to relatively crude assumptions. The relation between air speed, vehicle speed and fan speed can be made more accurate by utilizing more complex relations between

static and dynamic pressures for instance. The input in the model for the fan is the fan speed directly, which could be converted to power usage.

The heater/chiller unit is very simplified as the heat transfer of the unit is assumed to be independent of the coolant temperature. The controller assumes that the unit can deliver a specific amount of heat transfer to the coolant at any time. If the unit were to be modelled as a temperature dependent heat pump; the efficiency of the unit would be impacted by changing temperatures. The current assumption could be achieved by having a lower level controller delivering the input demanded by the RHC.

Impact of the pumps on the system is in the model's current state modelled directly as the volumetric flows being the inputs. An improvement would be to convert the input signals to be the pump powers. That would require relating the pump power to the volumetric flow it generates. Either white box or black box modelling could be utilized to derive transfer functions for the relations.

Another relevant assumption to investigate and review is that valve positions determine the direction of the flow. In reality this could be heavily dependent on pressure gradients in the thermal loops. This would also create new dependencies between the pump speeds and the valve positions.

An important aspect regarding the input signals that is not considered is that there is in fact relations between the inputs and the heat generated by the battery. Using electric power to chill or heat the coolant, driving the pumps and the fan does in fact use power that in turn heats the ESS.

5.2 Cost function tuning weights

The second research question regarding the cost terms is less clear from the current results. It is possible from the current model to heuristically tune the weights to give satisfactory performance even if the cost function of the optimization problem in its current state contains a mix of different units (rate of heat , fan speed, volumetric flow, temperatures). If the modelling improvements suggested above are implemented the cost function could naturally be formulated with a common unit for the system inputs, that being electric power. Minimization of battery usage would then better be represented in the cost function and thence tuning for real world scenarios facilitated. In addition, the cost function could benefit by being split into two parts; one containing the energy usage and the other punishing reference deviation. The two parts could as such receive focus in different areas. The energy minimization to be customized better to reflect battery usage, and the reference deviation be tied to component aging in a clearer way.

5.3 Control strategy

The structure of the model and controller could be fundamentally changed. The main principle that motivates the following ideas is that there is a time constant discrepancy. The ESS and MDS temperature dynamics are much slower than the coolant temperatures. Several ways to iterate on the current controller design are discussed.

5.3.1 Split horizon

One idea is to separate the receding horizon control into two prediction horizons. The slower states (ESS and MDS) would then be subject to a longer horizon and the faster states (coolants) to a shorter horizon. This approach has been implemented in OCPs before [28][29]. A benefit of this approach is to waste less computational resources on states that barely change in each iteration, and instead focus on the faster states.

5.3.2 Model simplification

Another approach is one suggested by the supervisor: to change the assumptions in the model itself. By, for example, assuming that the control volumes are equal to zero the coolant temperatures then become infinitely fast. It is then possible to split the problem into two separate controllers: One slow dynamics controller, considering the ESS and MDS that neglects the coolant water dynamics, and one fast dynamics controller, considering the coolant temperatures and regarding them as load disturbances. The fast controller decisions are then used as actuator signals for the slow dynamics. The approach would simplify the problem while reducing computational resources needed. The control system could, as knowledge about different modelling and control strategies develop, set the identified subsystems on different levels of control. This methodology of establishing a control hierarchy is very common in process control in industry utilizing what is called SCADA (Supervisory Control And Data Acquisition) [30]. A complete control system is constructed with control hierarchy in focus. Higher level model predictive controllers typically send setpoints to several lower level basic controllers (such as PIDs). An example the examiner suggested is to implement a lower level controller that can supply a certain rate of heat transfer from the coolant to the radiator, as the heater/chiller is currently modelled.

5.3.3 GSP comparison

The simulations assume some disturbance vectors that generate a new value every 300 seconds. An improvement to the simulations would be to utilize heat generation trajectories from accurate real-world drive cycles.

5.4 Conclusions

Simulating the complete thermal system using a receding horizon control strategy shows compelling potential benefits and opportunities for future improvement. The receding horizon controller has potential to lessen energy usage while improving reference tracking. The cost function has certain drawbacks that can be improved by advancing the modelling of the actuator signals. The overall mathematical model structure is a good starting ground for additional refinements in both the modelling of the system components and the development of control strategies.

Bibliography

1. Romijn T, Donkers M, Kessels JT, and Weiland S. Complete vehicle energy management with large horizon optimization. *2015 54th IEEE Conference on Decision and Control (CDC)*. IEEE. 2015 :632–7
2. Previati G, Mastinu G, and Gobbi M. Thermal Management of Electrified Vehicles—A Review. Energies 2022; 15:1326
3. Qureshi O and Armstrong P. Near-Optimal Receding Horizon Control of Thermal Energy Storage. Journal of Energy Resources Technology 2022; 144
4. Emilsson E and Dahllöf L. Lithium-ion vehicle battery production-status 2019 on energy use, CO2 emissions, use of metals, products environmental footprint, and recycling. 2019
5. Wöhrl K, Geisbauer C, Nebl C, Lott S, and Schweiger HG. Crashed electric vehicle handling and recommendations—state of the art in Germany. Energies 2021; 14:1040
6. Pardo-Ferreira MC, Torrecilla-Garcıa JA, Heras-Rosas CdL, and Rubio-Romero JC. New risk situations related to low noise from electric vehicles: perception of workers as pedestrians and other vehicle drivers. International journal of environmental research and public health 2020; 17:6701
7. Moazzen S, Razavian M, and Ghourchi M. Compiling Sustainable Urban Environmental Strategies with an Emphasis on the Industrial Sector; Case Study: Automotive Industry. Geographical Planning of Space 2020; 10:219–32
8. Elliott J and Lira C. Introductory chemical engineering thermodynamics. Prentice Hall, 2012
9. Incropera F, DeWitt D, Bergman T, and Lavine A. Chapter 1 - Fundamentals of heat and mass transfer. John Wiley & Sons; 2006
10. Welty J, Rorrer G, and Foster D. Chapter 14 - Fundamentals of momentum, heat and mass transfer, 6th edition international student version. John Wiley & Sons; 2014
11. Couper JR, Penney WR, Fair JR, and Walas. SM. Chapter 8 - Heat Transfer and Heat Exchangers. Gulf Professional Publishing, 2005
12. Incropera F, DeWitt D, Bergman T, and Lavine A. Chapter 11 - Fundamentals of heat and mass transfer. John Wiley & Sons; 2006
13. Titov G and Lustbader JA. Modeling control strategies and range impacts for electric vehicle integrated thermal management systems with MATLAB/Simulink. Tech. rep. National Renewable Energy Lab.(NREL), Golden, CO (United States), 2017
14. Lundgren J, Ronnqvist M, and Varbrand P. Chapter 1 - Optimization. Studentlitteratur; 2010

15. Diaz Dorado A. Efficient Convex Quadratic Optimization Solver for Embedded MPC Applications. 2018
16. Diehl M and Gros S. Chapter 1 - Numerical optimal control. Optimization in Engineering Center (OPTEC); 2011
17. Diehl M and Gros S. Chapter 8 - Numerical optimal control. Optimization in Engineering Center (OPTEC); 2011
18. Kelly M. Transcription methods for trajectory optimization: a beginners tutorial. Cornell University, 2017
19. Rantil J, Åkesson J, Führer C, and Gäfvert M. Multiple-Shooting Optimization using the JModelica. org Platform. *Proceedings of the 7th International Modelica Conference; Como; Italy; 20-22 September 2009*. 043. Citeseer. 2009 :757–64
20. Andersson JAE, Gillis J, Horn G, Rawlings JB, and Diehl M. CasADi – A software framework for nonlinear optimization and optimal control. Mathematical Programming Computation, 2018
21. Elhesasy M, Dief TN, Atallah M, Okasha M, Kamra MM, Yoshida S, and Rushdi MA. Non-Linear Model Predictive Control Using CasADi Package for Trajectory Tracking of Quadrotor. Energies 2023; 16:2143
22. Xu X, Yuan Y, and Dubljevic S. Receding horizon optimal operation and control of a solar-thermal district heating system. AIChE Journal 2018; 64:1217–33
23. Rawlings J, Mayne D, and Diehl M. Model predictive control: Theory, computation, and design. Nob Hill Publishing, 2017
24. Coron JM, Grüne L, and Worthmann K. Model predictive control, cost controllability, and homogeneity. SIAM Journal on Control and Optimization 2020; 58:2979–96
25. Jia Y, Jibrin R, and Görges D. Energy-optimal adaptive cruise control for electric vehicles based on linear and nonlinear model predictive control. IEEE Transactions on Vehicular Technology 2020; 69:14173–87
26. Gustafsson J. Linearization Based Model Predictive Control of a Diesel Engine with Exhaust Gas Recirculation and Variable-Geometry Turbocharger. 2021
27. Mattingley J, Wang Y, and Boyd S. Code generation for receding horizon control. *2010 IEEE International Symposium on Computer-Aided Control System Design*. IEEE. 2010 :985–92
28. Zlotnik D, Di Cairano S, and Weiss A. MPC for coupled station keeping, attitude control, and momentum management of GEO satellites using on-off electric propulsion. *2017 IEEE Conference on Control Technology and Applications (CCTA)*. IEEE. 2017 :1835–40
29. Hu Q, Amini MR, Wang H, Kolmanovsky I, and Sun J. Integrated power and thermal management of connected HEVs via multi-horizon MPC. *2020 American Control Conference (ACC)*. IEEE. 2020 :3053–8
30. Teaching Process Control Using SCADA Technology. IFAC Proceedings Volumes 2006; 39. 7th IFAC Symposium on Advances in Control Education:620–5

A

Appendix 1

The linearized system matrices used for the stability and controllability analysis.

$$\frac{df}{dx} = \begin{bmatrix} \frac{-(\alpha_{env}^{B} + \epsilon_B C_B)}{m_B C_{p,B}} & 0 & \frac{\epsilon_B C_B}{m_B C_{p,B}} & 0 \\ 0 & \frac{-(\alpha_{env}^{M} + \epsilon_M C_M)}{m_M C_{p,M}} & 0 & \frac{\epsilon_M C_M}{m_M C_{p,M}} \\ 0 & \frac{u_5 \epsilon_M C_M}{\rho_c V_1 C_{p,c}} & \frac{\epsilon_M C_B (u_5 - 1)}{\rho_c V_1 C_{p,c}} - \frac{u_5 u_3}{V_1} & \frac{u_5 (u_3 - \frac{\epsilon_M C_M}{\rho_c C_{p,c}})}{V_1} \\ \frac{u_5 \epsilon_B C_B}{\rho_c V_5 C_{p,c}} & \frac{(1-u_5)\epsilon_M C_M}{\rho_c V_5 C_{p,c}} & \frac{u_5 (u_3 - \frac{\epsilon_B C_B}{\rho_c C_{p,c}})}{V_5} & \frac{(u_5 - 1)\epsilon_M C_M}{\rho_c V_5 C_{p,c}} - \frac{u_5 u_3}{V_5} \end{bmatrix}$$

The 4x6 input matrix jacobian matrix is split into two parts to fit the report. The first three columns;

$$\frac{df}{du}(:, 1:3) = \begin{bmatrix} \frac{\epsilon_B C_B}{\rho_c m_B f_B C_{p,c} C_{p,B}} & 0 & \frac{-\dot{Q}_{ch} \epsilon_B C_B}{\rho_c u_3^2 m_B C_{p,c} C_{p,B}} \\ 0 & 0 & 0 \\ \frac{(\epsilon_B C_B (\frac{1}{\rho_c u_3 C_{p,c}} - 1) - 1)(u_5 - 1)}{\rho_c V_1 C_{p,c}} & \frac{u_5 u_6}{\rho_c V_1 C_{p,c}} & \frac{-u_5 (x_3 - x_4)}{V_1} - \frac{(u_5 - 1)\epsilon_B C_B u_1}{\rho_c^2 u_3^2 V_1 C_{p,c}^2} \\ -u_5 \frac{(\frac{\epsilon_B C_B}{\rho_c u_3 C_{p,c}} - 1)}{\rho_c V_5 C_{p,c}} & \frac{(1-u_5) u_6}{\rho_c V_5 C_{p,c}} & \frac{u_5}{V_5}(x_3 - x_4 + \frac{\epsilon_B C_B u_1}{\rho_c^2 u_3^2 C_{p,c}^2}) \end{bmatrix}$$

Followed by the last three columns:

$$\frac{df}{du}(:, 4:6) = \begin{bmatrix} 0 & 0 & 0 \\ 0 & 0 & 0 \\ 0 & -\frac{1}{V_1}(u_3(x_3 - x_4) - \frac{u_6 \dot{Q}_r - \epsilon_M C_M (x_4 - x_2)}{\rho_c C_{p,c}}) - \frac{u_1 - \epsilon_B C_B (x_3 - u_1 + \frac{u_1}{\rho_c u_3 C_{p,c}})}{\rho_c V_1 C_{p,c}} & \frac{u_5 \dot{Q}_r}{\rho_c V_1 C_{p,c}} \\ 0 & \frac{1}{V_5}(u_3(x_3 - x_4) + \frac{u_1 - \epsilon_B C_B (x_3 - x_1 + \frac{u_1}{\rho_c u_3 C_{p,c}})}{\rho_c C_{p,c}}) - \frac{u_6 \dot{Q}_r - \epsilon_M C_M (x_4 - x_2)}{\rho_c V_5 C_{p,c}} & \frac{(1-u_5)\dot{Q}_r}{\rho_c V_5 C_{p,c}} \end{bmatrix}$$

And lastly the disturbance jacobian matrix;

$$\frac{df}{dv} = \begin{bmatrix} \frac{1}{m_B C_{p,B}} & 0 & \frac{\alpha_{env}^{B}}{m_B C_{p,B}} \\ 0 & \frac{1}{m_M C_{p,M}} & \frac{\alpha_{env}^{M}}{m_M C_{p,M}} \\ 0 & 0 & 0 \\ 0 & 0 & 0 \end{bmatrix}$$

DEPARTMENT OF ELECTRICAL ENGINEERING
CHALMERS UNIVERSITY OF TECHNOLOGY
Gothenburg, Sweden
www.chalmers.se

CHALMERS
UNIVERSITY OF TECHNOLOGY